MICROCANTILEVER BASED VISCOSITY MEASUREMENT AS IT APPLIES TO OSCILLATION AMPLITUDE RESPONSE

Sanford H. Siegel III

Thesis Prepared for the Degree of

MASTER OF SCIENCE

UNIVERSITY OF NORTH TEXAS

August 2018

APPROVED:

Tae-Youl Choi, Major Professor
Haifeng Zhang, Committee Member
Xiaohua Li, Committee Member
Kuruvilla John, Chair of the Department of Mechanical and Energy Engineering
Yan Huang, Interim Dean of the College of Engineering
Victor Prybutok, Dean of the Toulouse Graduate School

Siegel III, Sanford H. *Microcantilever Based Viscosity Measurement as It Applies to Oscillation Amplitude Response*. Master of Science (Mechanical and Energy Engineering), August 2018, 71 pp., 29 tables, 66 figures, 35 numbered references.

The goal of this research is to measure viscosity via the analysis of amplitude response of a piezo driven vibrating cantilevers partially immersed in a viscous medium. As a driving frequency is applied to a piezoceramic material, the external forces acting on the system will affect its maximum amplitude. This thesis applies this principle through experimental and analytical analyses of the proportional relationship between viscosity and the amplitude response of the first natural frequency mode of the sinusoidal vibration.

Currently, the few cantilever-based viscometer designs that exist employ resonant frequency response as the parameter by which the viscosity is correlated. The proposed piezoelectric viscometer employs amplitude response in lieu of resonant frequency response. The goal of this aspect of the research was to provide data confirming amplitude response as a viable method for determining viscosity. A miniature piezoelectric plate was mounted to a small stainless-steel cantilever beam. The tip of the cantilever was immersed within various fluid test samples. The cantilever was then swept through a range of frequencies in which the first frequency mode resided. The operating principle being as the viscosity of the fluid increases the amplitude response of cantilever vibration will decrease relatively. What was found was in fact an inversely exponential relationship between dynamic viscosity and the cantilever beam's vibrational amplitude response. The experiment was performed using three types of cantilevers as to experimentally test the sensitivity of each.

ACKNOWLEDGMENTS

Firstly, I would like to convey my gratitude toward Dr. Tae-Youl Choi for his guidance and support. He pushed me to achieve goals past what I even dreamed possible. His assistance with providing me the contacts required to make the cantilevers was invaluable and I am deeply grateful.

I also would like to acknowledge Mr. Chen Zhang, PHD student in the department of Mechanical Engineering at the University of North Texas. Without his daily support this project would not have been possible. He guided me when necessary as well as helped me up the learning curve with the scientific equipment. I am also grateful for his expertise lending me his experience with physically crafting the cantilevers used in this experiment.

I also can't go without acknowledging Dr. Haifeng Zhang, Professor in the Mechanical Engineering Department. His expertise on the subject of vibration as well as piezoelectricity itself proved to be a great help with the theoretical as well as the experimental data was imperative to the completion of this research. I would also like to thank him for the use of his lab and equipment necessary for the completion of this project.

I wish to also acknowledge Dr. Jianchao Li, Professor in the Materials Science department at the University of North Texas. I am indebted to him for manufacturing a new electrode for the PZT-5H used for the cantilevers.

TABLE OF CONTENTS

Page

LIST OF TABLES

Page

LIST OF FIGURES

Page

NOMENCLATURE

ΔP	Pressure Difference
BNC	Bayonet Neill Concelman connector
DC	Direct Current
CNC	Computer Numerical Control
DOF	Degree of Freedom
Hz	Hertz
LASER	Light Amplified by Stimulated Emission of Radiation
Mm	millimeter
ODE	Ordinary Differential Equation
PDE	Partial Differential Equation
POC	Percent of Change
PSIG	Pounds per Square Inch Gauge Pressure
SAE	Society of Automotive Engineering
um/v	micrometer per volt

CHAPTER 1

INTRODUCTION

1.1 Overview of Microcantilever Viscometer

Knowing the viscosity of a fluid is often critical when designing and operating mechanical systems. Devices for measuring viscosity (known as viscometers) are extremely important both commercially as well as in the laboratory setting. Most viscometers are large, intrusive, cumbersome devices. The advantage of vibrational based viscometers is they can be made much smaller and much less intrusive than conventional viscometers. The use of vibration as a means of determining viscosity is not a recent one. Research around cantilever-based viscometers date back to the 1950's Bendix Instrument [2]. The United States Air force was also performing research in this area as far back as 1972 [1]. The basic principle behind vibrational type viscometers is as they oscillate, the surrounding fluid affects the vibrational characteristics of the oscillatory body. The change of these characteristics directly reflects the viscosity and density of the fluid. By measuring the changes in the vibrational characteristics, one can ascertain the viscosity. Historically, the vibrational characteristic correlated to viscosity is resonance frequency.

The goal of this research is measure viscosity via the analysis of amplitude response of a piezo driven vibrating cantilevers partially immersed in a viscous medium. A thin 301 stainless-steel cantilever under fixed free conditions was chosen as the oscillating body for experimentation. The free end (tip) of the cantilever was immersed 4mm into different oil samples of various viscosities (Fig 1.1.). As the cantilever oscillated, the fluid produced a viscous drag force on the immersed tip. An American Piezo brand PZT-5H piezoceramic is

attached near the fixed end of the cantilever to drive the vibration. The piezo was driven over a range of frequencies containing the piezo-cantilever system's first mode resonance frequency.

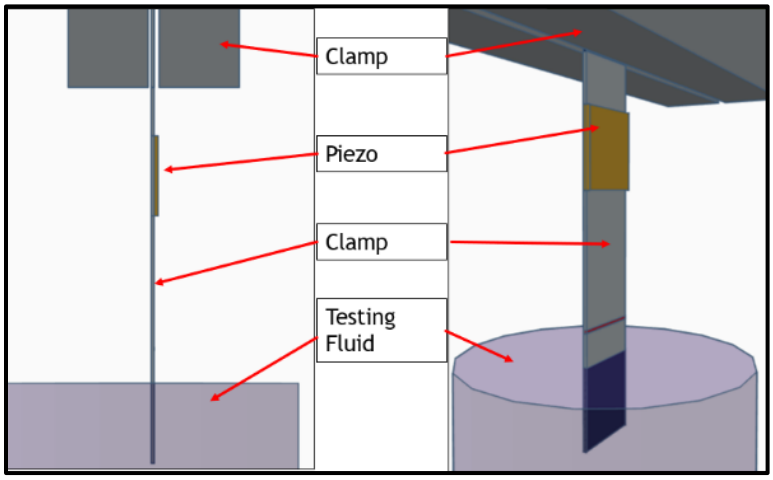

Figure 1.1: Viscometer Overview Reference Diagram

The displacement of the system was tracked optically using a Polytec OFV-505 laser vibrometer and associated Polytec OFV-5000 Vibrometer Controller. The output of the vibrometer controller was fed to LabView creating a displacement graph over the range of frequencies. The data for each test was exported from LabView to an excel workbook. As the viscosity of the testing sample increased the displacement amplitude of the cantilever decreased in a negative exponential curve. Therefore, it can be said that the cantilever's amplitude directly corresponds to the viscosity of the fluid sample.

Three different cantilevers were tested during the experiment to ascertain which yielded the best sensitivity. The cantilevers of (Fig 1.2.) depict the three cantilevers types used in this experiment along with section descriptions. The reference names used for each cantilever (from left to right) are "zero-step", "one-step", and "two-step. This naming convention remains consistent throughout the rest of this paper. Each stainless-steel cantilever is clamped on one end leaving 18 mm of free length to the tip (Fig 1.2.). The displacement was measured at position (X=12mm) as measured from the clamping surface for each cantilever.

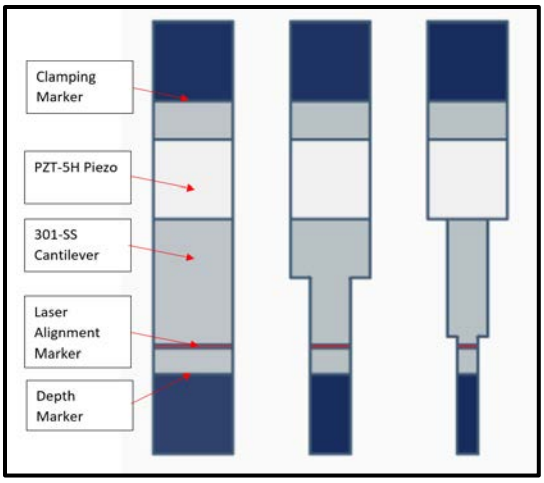

Figure 1.2: Cantilever Specimen Reference Diagram

(As Referenced From Clamping Mark)	Zero-Step (Left)	One-Step (Middle)	One-Step (Middle)
Section One: Length (mm)	18	9	6
Section One: Width (mm)	4	4	4
Section Two: Length (mm)	N/A	9	6
Section Two: Width (mm)	N/A	2	2
Section Three: Length (mm)	N/A	N/A	6
Section Three: Width (mm)	N/A	N/A	1

Table 1.1: Cantilever Specimen Dimension Reference Table

1.2 Literature Survey

This section briefly describes the results of the literature review performed prior to embarking on the experiment. Basic concepts of piezoelectricity are first discussed. Viscometers of all types are briefly reviewed. Lastly literature pertinent to this research is reviewed.

1.2.1 Physical Properties

A piezo is an electrical device that when deformed or compressed creates an electrical current. Direct current will either compress or expand the piezo depending on the polarity of the

induced charge. When an alternating current is applied the piezo will contract and expand at the frequency of the alternating current. For example, if 60hz is applied to the piezo it will vibrate at 60hz. Like most electrical devices the piezoelectric process is reversible such as in an electric motor. When an electric motor armature is rotated it will create an electrical current. A piezo behaves the same way, when voltage is applied to a piezo it will compress or deform. This scientific journal focuses on ceramic type piezoelectric devices as this is what was used. [26]

Piezoelectricity is a phenomenon with a myriad of uses. These uses include engine knock sensors, pressure sensors, electric toothbrushes, ultrasonic cleaners, instrument pickups, and most commonly cellphone and earbud speakers. [26]

For a material to display piezoelectric properties it must possess certain properties. A piezoelectric material must be anisotropic elastic as well as be anisotropic dielectric where both properties are coupled. The material must also be able to be polarized. The aforementioned properties are discussed in the subsequent paragraphs. [26]

The first of these characteristics to be discussed is anisotropic elasticity. As counterintuitive as it may seem, piezoelectric materials such as ceramic or quartz have elastic properties. Without elasticity a material, cannot deform. When it comes to elasticity, there are two types, anisotropic and isotropic. Isotropic elasticity defines a material that deforms evenly in all directions. A piezo however, is an anisotropic elastic material, meaning piezoelectric materials deform differently in one direction than all others. An example of anisotropic elasticity is wood. The elasticity of wood along different axis depends on if the elasticity is being measured parallel or perpendicular to the grain structure. It is therefore imperative to consider anisotropic elasticity when making calculations for piezoelectric materials as calculations for isotropic materials are much different. [25], [26]

Polarization in this context refers to forcibly moving the positive and negative electrical charges to opposing sides of the material being polarized, thus creating a dipole. A dipole as it applies to a piezo is defined as a pair of oppositely charged poles of equal magnitude (depicted as the red and blue spheres in (Fig 1.3)). Synthetic piezoelectric materials such as piezoceramics require polarization. [25], [26]

Polarization of a piezoceramic material is the process by which the dipoles are roughly aligned along one axis using a strong electrical field. A ceramic type piezo consists of two metal electrodes with the piezoceramic material sandwiched between. The poling axis is perpendicular to the surface of the electrodes (top and bottom surfaces of (Fig 1.2).

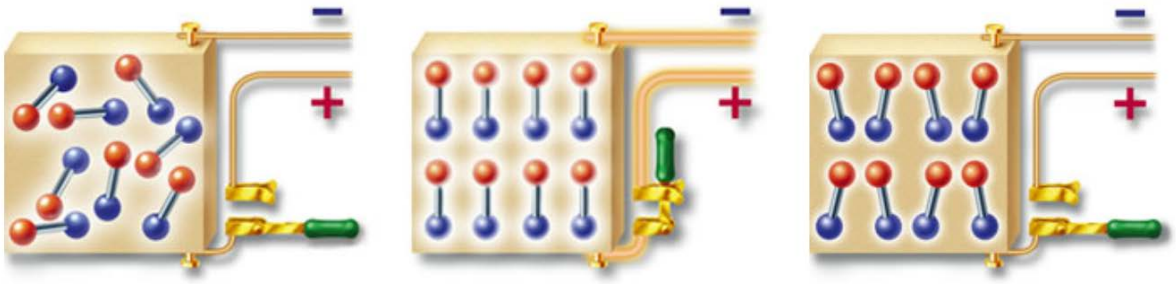

Figure 1.3: Piezoceramic Dipole Polarization Process Diagram (Before-Left, During-Middle, After-Right) [25]

In (Fig 1.3.) the leftmost diagram represents the material before polarization; the charges within the material are randomly aligned and the circuit is open. The middle picture of (Fig 1.3.) shows the material during polarization; the circuit is closed, and the dipoles are aligned to the applied DC (direct current) electric field. Note that in (Fig 1.3.) the positive poles align to the negative (top) electrode and the negative charges align to the positive (bottom) electrode. Between the middle and rightmost stage of the polarization process one might inquire as to how the dipoles themselves stay locked into their new position. To answer this question, it is necessary to briefly discuss the process by which a piezoceramic material is created. The

piezoceramic material starts off as a powder containing the specific metal oxides of the piezoceramic being created. The powder is then fired to sinter the powder into a crystalline structure. Sintering is the process by which a powder is heated to a point where it coalesces without heating it to the point where it liquifies. Once sintered, the material is then formed into the desired final piezoceramic shape and the electrodes are applied. This stage is depicted in the leftmost diagram of (Fig 1.3.). The material is then reheated past what is known as the Curie point. As the material is heated an electrical field density of 10^6 V/m is applied to the electrodes to align the dipoles in approximately same direction. The process by which this happens is called spontaneous polarization and is depicted in the middle diagram of (Fig 1.3.). The material is then cooled, thus locking the dipoles in place. The rightmost diagram of (Fig 1.3.) has the circuit open as at this stage the applied electrical field is no longer necessary because the pertinent dipole had been created [5]. Lastly, the rightmost diagram shows the dipoles aren't perfectly aligned with the poling axis. This is no accident, if the dipoles were perfectly aligned the piezo would not function. The slight amount of misalignment allows for the piezo to deform by using the dipoles to exert toque on the material as an electrical field is applied. [25], [26]

A piezoelectric material must also be dielectric. A dielectric material (Fig 1.4.) is a material that will support an electrical charge, however that property alone doesn't make a material dielectric. For a material to be dielectric it must have little to no free electrical charges. In other words, a dielectric material has a near infinite electrical resistance while still being able to support an electrical charge. Instead the charges are shifted from their rest position thus polarizing the dielectric material. This property is also important for capacitors. In a capacitor the dielectric material is sandwiched between two metal plates. Once charged, the capacitor maintains an electron imbalance until discharged. For a dielectric material to be piezoelectric it

must be a special type of dielectric called an anisotropic dielectric. Much like anisotropic elasticity, an anisotropic dielectric has an electric charge in one direction or along one axis (the poling axis). [25], [26],[34]

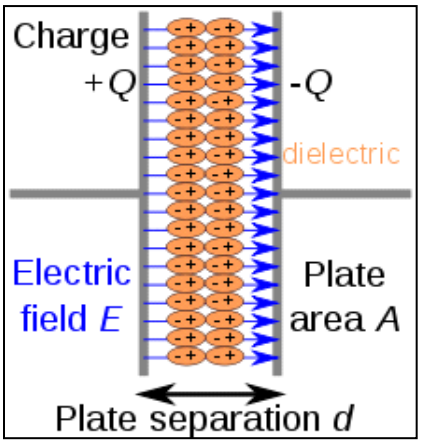

Figure 1.4: Dielectric Reference Diagram [34]

The understanding of piezoelectric devices first requires a foreknowledge of several concepts and properties. Stress "T" is defined as the force per unit area of the applied force. Stress is often given in units of pascals (Pa) which is equivalent to one newton per meter squared or alternatively in pounds per square inch in imperial units. Stress in piezoelectric materials can either be caused by deformation due to an applied electrical field or of an external force applied thus creating an electrical charge. It is also worth discussing sign convention as it applies to stress. Generally, a material under tension is deemed to have a positive stress, whereas under compression it is negative. [25], [26]

Strain is often an accompanying concept when discussing stress with the two terms being proportional. Strain is the deformation of a material along a particular direction divided by the original length of the material along that same direction due to an applied stress. In other words, strain is the change in length divided by the original length and as such is dimensionless. [26]

As piezos are electrical devices the concept of an electric field “E” is applicable. For the purposes of this research in depth explanation of electric fields is not required. An electrical field is simply the voltage per meter (either direct current (DC) or alternating current (AC)) that is applied to the piezoelectric material. The unit of volts per meter is a way of quantifying the intensity of the electrical field based on the voltage between two points one meter apart. [26]

The piezoelectric constant “d” is a ratio that changes definition based on whether an electric charge is being applied or produced. Due to the reversable nature of piezoelectric materials this constant is defined in two ways. When applying an electric field, the piezoelectric constant is termed the piezoelectric “charge” constant with units of meters per volt. The piezoelectric charge constant relates stress and the applied electric field. Conversely, when the piezoelectric material is being mechanically deformed and producing an electric field, it is called the piezoelectric “deformation” constant. The piezoelectric deformation constant relates the electrical charge produced to the mechanical stress with units of Coulombs per Newton. [26]

Permittivity “ε” is yet another important concept required for the understanding of piezoelectric materials. Permittivity in this context refers to the ability of the piezoelectric material to store either electrical or mechanical energy depending on whether the electricity is being applied or produced with units of farads per meter. [26]

Equations 1.1-1.4 are arguably the most common forms of the piezoelectric constitutive equations and are referred to as linear constitutive equations. They are most commonly used for finite element analysis (FEA). [26]a

$$S = s^{E} * T + [d]^{t} * E \qquad \text{Equation 1.1}$$

$$D = d * T\varepsilon^{T} * E \qquad \text{Equation 1.2}$$

Equations 1.1-1.2 are the equation forms used when an electric field is being applied. The

s^E term is the elastic compliance (Strain/Stress) during the closed-circuit condition. The superscript "t" on the $[d]^t$ term simply indicates a matrix transpose during calculation. The superscript "T" on the ε^T term denotes permittivity as it relates to stress. [26]

$$S = s^D T + [g]^t D \quad \text{Equation 1.3}$$

$$E = -gT + [\varepsilon^T]^{-1} D \quad \text{Equation 1.4}$$

Conversely, equations 1.3-1.4 are the equivalent forms when the piezoelectric material is being mechanically deformed and producing an electrical field. The s^D term is the elastic compliance (Strain/Stress) during the closed-circuit condition. As with equations 1.1-1.2, the superscript "t" on the $[g]^t$ term simply indicates a matrix transpose during calculation. The "g" in the $[g]^t$ term represents the piezoelectric voltage coefficient. This can simply be thought of as the "d" equivalent of this case. Again, the superscript "T" on the ε^T term denotes permittivity as it relates to stress. [26]

1.2.2 Overview of Viscometers

Viscosity is a fluid dynamics property that quantifies a fluids resistance to flow. There are two methods of quantifying viscosity, kinematic and dynamic. Conceptually, dynamic (also known as absolute) viscosity is a measure of tangential force required to move one plate past another parallel stationary plate given a fixed gap distance and velocity (Figure 1.5.).

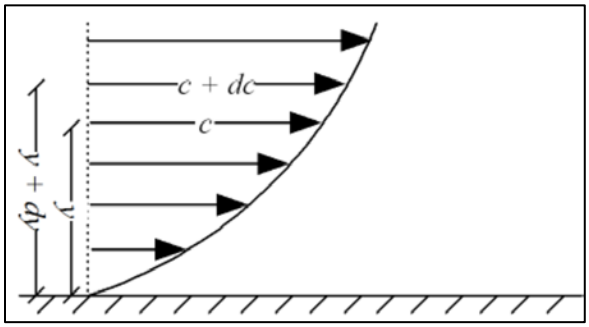

Figure 1.5: Diagram of Kinematic Viscosity Definition [15]

The quantification of dynamic viscosity requires the fluid to be in the laminar flow regime as well as the fluid to be Newtonian.

$$\mu = \tau * dc/dy \qquad \text{Equation 1.5}$$

where:

$\mu = \text{dynamic viscosity } (kg/ms)$

$\tau = \text{fluidic shear stress}(N/m^2)$

$dc = \text{unit velocity}(m/s)$

$dy = \text{unit distance between layers}(m)$

Kinematic viscosity is simply a modification of dynamic viscosity. Kinematic viscosity is simply dynamic viscosity divided by the density of the fluid in question.

$$v = \mu/\rho \qquad \text{Equation 1.6}$$

where:

$v = \text{kinematic viscosity}(m\text{^}2/s)$

$\mu = \text{dynamic viscosity } (kg/ms)$

$\rho = \text{density of fluid}(kg/m\text{^}3)$

The above equations were not directly used for the purposes of this research. However, it is necessary to research the concept and differences between dynamic and kinematic viscosity for the purposes understanding their application. Dynamic viscosity was what was used in this research. [15], [26]

There are quite a few techniques and devices for measuring viscosity. Most of these devices historically relied on non-vibrational techniques. These techniques are only briefly discussed in the subsequent sections as this research involves vibration related techniques for measuring viscosity, this area is much more relevant and is discussed in further detail.

U-Tube viscometers are very simple devices (Fig 1.6.). Also called Ostwald viscometers, was invented by Wilhelm Ostwald. The operating principle involves recording time it takes for fluid to flow from one area to another due to gravity. A specific version of the U-tube viscometer used for high viscosity fluids, called a Ubbelohda Viscometer, places the U-Tube in a temperature-controlled bath to lower the viscosity to allow for measurement. The fluid is sucked up to fill the upper bulb. Once the suction is released the fluid travels through the capillary tube below marker D to the lower bulb. The time it takes for the surface up the fluid to translate from line C to line D is measured. The time it takes the fluid to travel between these two markers is directly proportional to kinematic viscosity. The calibration factor of the U-Tube viscometers can be derived using the manufacturers specifications or by calculating it from a fluid of known viscosity. [16], [20]

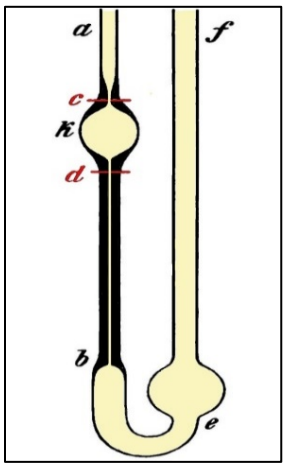

Figure 1.6: U-Tube Viscometer [20]

Another very common method for determining viscosity is termed the Falling Sphere. The sphere is placed inside a transparent tube filled with the tested fluid. Two marks are placed toward the bottom of the tube as to allow the sphere to reach terminal velocity. In principle, the viscosity induced terminal velocity is calculated from the time required for the sphere to pass between the two marked points at the spheres terminal velocity. As terminal velocity is the point

at which the force of gravity equally opposes the viscous drag force (Fig 1.7.), a higher viscous drag force results in a lower terminal velocity. Therefore, the terminal velocity of the sphere is inversely proportional to dynamic viscosity. The viscous drag force induced on the sphere is calculated via Stokes-Law. As it turned out, a version of Stokes-Law was used for the purposes of this research (Section 2.2). [16]

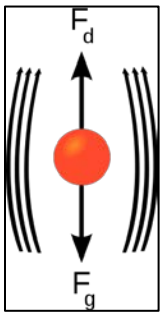

Figure 1.7: Falling Sphere Viscometer [20]

The Falling Piston viscometer, also known as the Norcross Viscometer, was invented by Austin Norcross. Although it may seem congruent to the Falling Sphere method, the theoretical principle is very different. While held in the up position (leftmost diagram (Fig 1.8.)), the fluid is drawn into the empty space below the piston. The piston is then released and falls due to gravity. The testing fluid flows toward the top of the piston via a specified clearance between the piston and cylinder. The time it takes for the piston to reach the bottom of the cylinder is proportional to the viscosity of the tested fluid. As the fluid moves through the clearance, it is slowed due to the shear stress of the fluid between a static cylinder and the moving piston. [16]

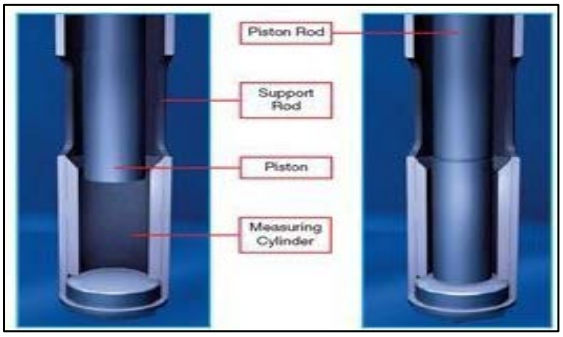

Figure 1.8: Falling Piston Viscometer [18]

Although distinctly different to the Falling piston method, the Oscillating Piston works via a very similar principle. Like the Falling Piston method, the Oscillating Piston measures viscosity based on a clearance induced fluidic shear stress between its piston and cylinder. The key difference is the piston is made to oscillate back and forth within the cylinder using electromagnets (Fig 1.9.). The time required for each oscillation cycle is then measured. The viscosity is therefore proportional to the length of time for each oscillation. [16], [17]

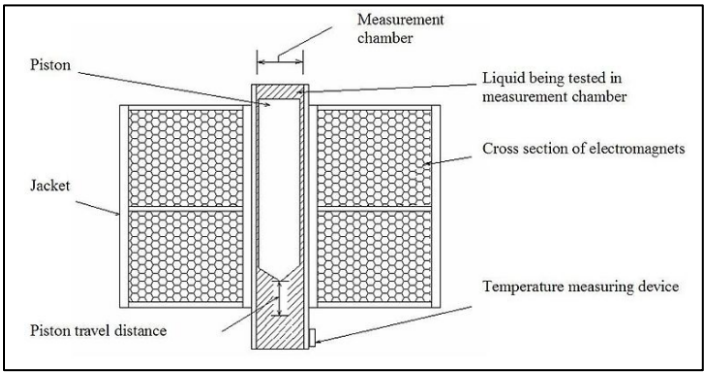

Figure 1.9: Oscillating Piston Viscometer [20]

The Bubble viscometer is arguable the most rudimentary means by which a viscosity measurement can be taken. However, that is not to imply extreme variances in accuracy. The fluid is placed within a vertical testing tube and sealed with a cork. The principle is simple, the time it takes for the bubble to pass between two marks on the testing tube is proportional to viscosity. The tested fluid is filled up to the 100 mm mark for the specific version depicted in (Fig 1.10.). This forms an air gap between the 100mm mark and the 108mm mark. After capping it off with a cork, the sample is oriented cork side down until the bubble formed by the air gap reaches the other side of the cylinder. The testing tube is then flipped cork side up. Lastly the time it takes the bubble to pass between the 27mm and the 108mm line is measured. The advantage of this method is it can be performed quickly cheaply, and simply. However, results may vary depending on the shape of the bubble formed. [19]

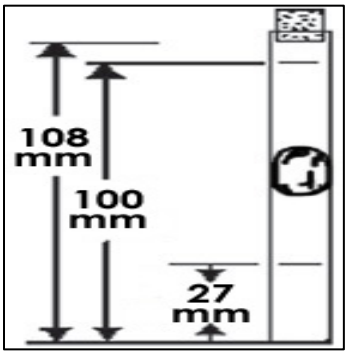

Figure 1.10: Bubble Viscometer [19]

Rotational Viscometers relate torque to viscosity through fluidic shear stress. A specific type of rotational viscometer is termed the “cup and bob” (Figure 1.11.). This consists of a rotating cylinder placed within a fixed cylinder filled with the tested fluid. As the cylinder rotates the torque required to overcome the fluidic shear stress is measured. The Torque and consequently shear stress, is proportional to viscosity. This type of viscometer is most commonly used as instrumentation. Other variants along this same principle include a rotating cone set close to a static plate as well as a rotating disk set near a static plate. [16], [20]

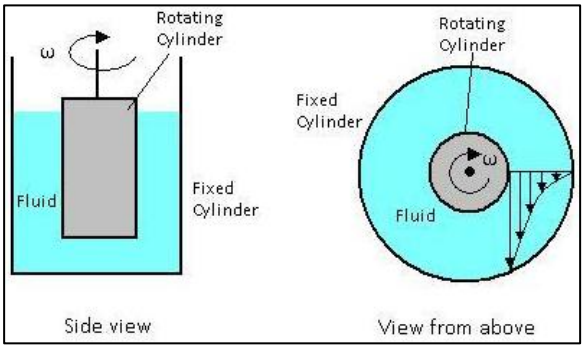

Figure 1.11: Rotating Viscometer [35]

1.2.3 Design Review

This section includes the relevant literature reviewed concerning the design of microcantilever viscometers. Topics include forced vibration techniques, various cantilever profiles, as well as different methods of cantilever fluid interaction.

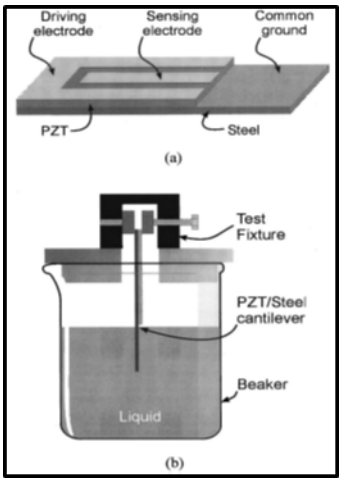

Figure 1.12: W. Shih et al. Cantilever [6]

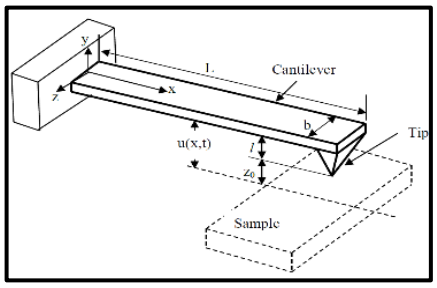

Figure 1.13: M. Salgar Cantilever [7]

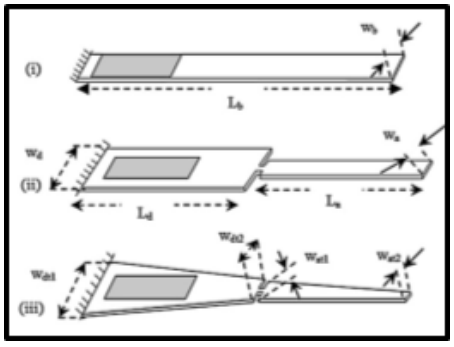

Figure 1.14: S. Sathiya et al. Cantilever [8]

W. Shih et al. [6] experimented with a unimorph cantilever made of a ceramic piezo and stainless steel. A thin cantilever was fabricated where its width is much less than its overall length. The cantilever then had the piezo mounted nearer to its clamping end to drive the vibration. The free end of the cantilever was immersed in the tested fluid. The driver and sensor were made to operate from the same piezo by dividing one electrode into separate sections (Fig 1.12). The resonant frequencies of the piezo-based sensor were then determined by use of an oscilloscope

M. Salgar [7] experimented with a cantilever design by which a pyramid shaped tip was attached facing down to a horizonal cantilever (Fig 1.13). Rather than the cantilever itself interacting with the fluid sample the perpendicular mounted pyramid-like tip provided the interaction.

S. Sathiya et al. [8] tested three different cantilever designs (Fig 1.14). The three different designs facilitated the comparison of cantilever sensitivity. The vibration was driven by a piezo mounted towards the clamping end of the cantilever. Each cantilever was tested with tips immersed in the testing fluid. The straight cantilever was analyzed as a 1-DOF vibration while the one step and trapezoidal cantilever were analyzed as 2-DOF

systems. The indentions between the two sections of these cantilevers served to provide an additional DOF.

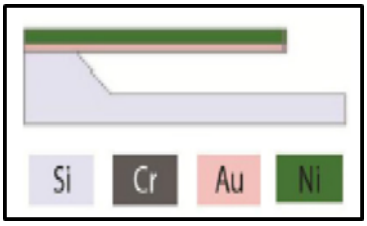

Figure 1.15: G. Eris et al. Cantilever [9]

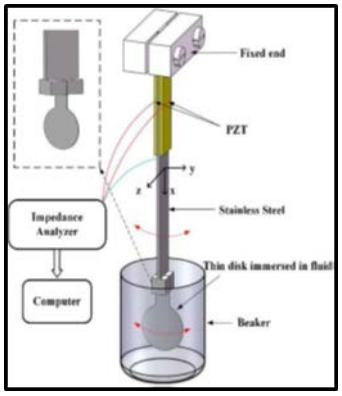

Figure 1.16: G. Wang et al. Cantilever [10]

G. Eris et al. [9] used a unique approach. The fixed-free cantilever design was made from layers of gold and nickel with a chromium coating and mounted on a silver base (Fig 1.15). What makes the methodology unique is a electromagnetic field was used to oscillate the cantilever. A field coil was constructed and connected to a waveform generator with an alternating current output.

G. Wang et al. [10] experimented with a bimorph cantilever design with its tip immersed in the testing fluid. The design employs two piezoceramic plates mounted on each side of the cantilever toward its clamping end. Uniquely, the tip is oriented with the major surface area oriented perpendicular to the cantilevers oscillation (Fig 1.16.). The cantilevers interaction with the testing fluid is primarily the shear stress of the fluid acting on its major surface areas.

1.2.4 Analytical Review

This section overviews literature reviewed over the various analytical methods performed in previous studies. Content includes the various analytical modeling methods involved in calculating the vibrational characteristics of cantilever beams.

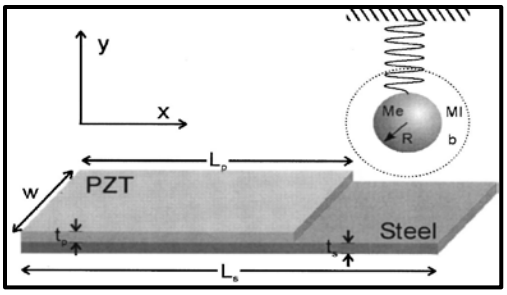

Figure 1.17: W. Shih et al. Analytical model [6]

W. Shih et al. [6] modeled their cantilever as an oscillating sphere. This technique models the cantilever as a spring mass system where the mass is a sphere (Fig 1.17.). The sphere is modeled as oscillating in a fluid. The attachment point of the coil spring is taken as an external harmonic force $F_0 e^{-i\omega t}$. The effects of viscous drag force are then calculated using Stokes-Law.

C. Riesch et al. [12] calculated resonant frequency via the Euler-Bernoulli beam theory equation as seen below. See (Fig 1.18.) for reference.

$$EI\left(\frac{d^4\big(w(x,t)\big)}{dx^4}\right)+\left(\frac{d^2\big(w(x,t)\big)}{dt^2}\right)=\left(\frac{d^2\left(M_p(x,t)\right)}{dt^2}\right)$$

where:

- $w(x,t)$: displacement of cantilever at position (x) and at time(t)
- E: The elastic modulus
- I: Second moment of inertia
- ρ: Density of the cantilever
- A: Cross sectional area of cantilever
- M_p=Moment due to piezoelectric force

Using Euler-Bernoulli beam in combination with Stokes-Law they were able to calculate resonant frequency

$$F_D = 6\pi\eta R v$$

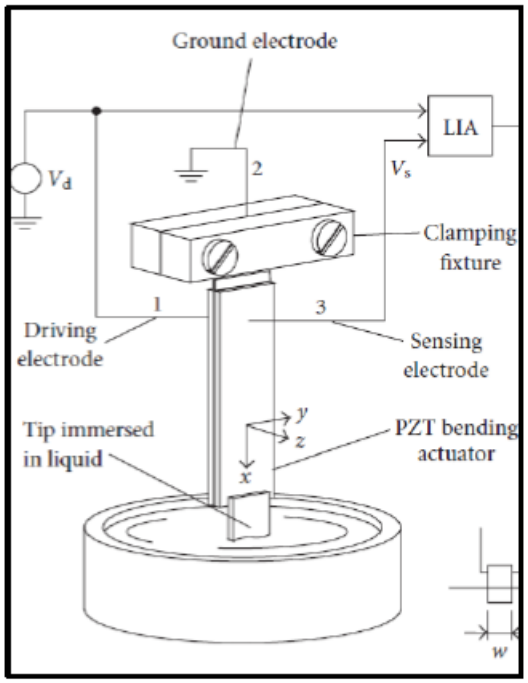

Figure 1.18: C. Riesch et al. Cantilever Design [12]

The force of drag (F_D) is calculated where η, ν, and R represent the dynamic viscosity, relative velocity of the cantilever tip, and equivalent radius of the cantilever tip respectively. The equivalent radius is typically found by equating the volume of the cantilever to a sphere. This method has proved to be an accurate way of determining the drag force on the tip of a vibrating cantilever while making theoretical calculations. A variation of this method was chosen as a reference for the analytical calculations of this report due to the similarity in design (Fig 1.17). Their method for measuring oscillation via a laser vibrometer was also adopted.

S. Boskovic et al. [13] researched the oscillation of a cantilever completely immersed in the testing fluid. The cantilever was modeled by approximating it as simple harmonic motion. The method by which they derived an equation to account for the hydrodynamic forces was via a transfer function within the harmonic excitation equation. Values for resonance frequency an quality factors required to solve their harmonic excitation model were experimentally derived

and therefore acted as calibration factors for their analytical calculation. This was done due to the complexity of solving a problem such as this.

1.3 Scope and Objective

The main objective of this research is to develop a piezoelectric viscosity sensor and evaluate its viability and sensitivity based upon amplitude change due to the drag force on the Microcantilever system as its tip oscillates through testing fluid. As a baseline the amplitude change will be evaluated against known viscosities of oil.

The specific objectives for this research are:

- Fabricate three piezoelectric microcantilever viscometers
- Calibrate the fabricated microcantilever viscometers amplitude change against known oil viscosities
- Compare the sensitivity between the three microcantilever viscometer designs
- Analyze the sensitivity of amplitude as it relates to viscosity verses frequency

CHAPTER 2

MATHEMATICAL MODELING

2.1 Known Viscosity Values

Mathematical modeling was performed to determine an equation to correlate cantilever viscosity to cantilever maximum displacement. The first step was to obtain a temperature verses viscosity graph for each of the oils tested.

	SAE-5W-20	SAE-30W	SAE-15W-40	SAE-10W-60
Temperature (in Celcius)	Dynamic Viscosity (mPa*s)	Dynamic Viscosity (mPa*s)	Dynamic Viscosity (mPa*s)	Dynamic Viscosity (mPa*s)
0.00	**347.17**	**1124.10**	**1328.00**	**1453.80**
10.00	**178.50**	**491.10**	**582.95**	**712.34**
20.00	**100.43**	**239.39**	**287.23**	**381.08**
30.00	**60.88**	**128.42**	**155.31**	**220.06**
40.00	**39.28**	**74.55**	**91.06**	**135.52**
50.00	**26.69**	**46.43**	**57.17**	**88.55**
60.00	**18.95**	**30.58**	**38.07**	**60.60**
70.00	**13.97**	**21.17**	**26.58**	**43.23**
80.00	**10.62**	**15.28**	**19.36**	**31.95**
90.00	**8.30**	**11.42**	**14.59**	**24.31**
100.00	**6.64**	**8.80**	**11.32**	**18.99**

Table 2.1: Dynamic Viscosity

For the purposes of this research the dynamic viscosity is the pertinent measurement to consider. (Table 2.1) displays the dynamic viscosity verses ambient temperature for testing samples used in the experiment. The testing samples include motor oil types: SAE10W-60, SAE15W-40, SAE30 and SAE5W-20. From these tables a scatter type plot was created using excel. A sixth order polynomial regression was chosen as the best “Fit” for the excel data. The

trendline itself was automatically “fitted” via Microsoft Excel (Fig. 2.1). The resulting sixth order polynomial was then used to calculate the viscosity at the specific room temperature of the testing environment (23 Celsius) (Table 2.2.). REF [11], [29]

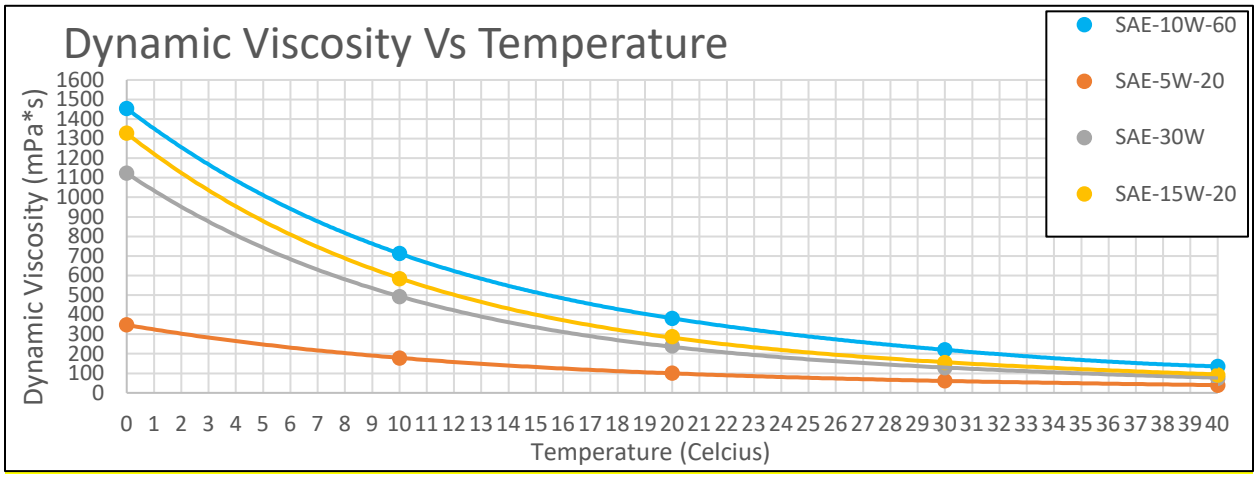

Figure 2.1: Dynamic Viscosity vs. Temperature Trendline Fit

Testing Fluid	Sixth Order Polynomial Regression Trendline Equations	Dynamic Viscosity (mPa*s) (x-value @23 Celcius)
SAE-5W-20	$y = 0.0001313170x^4 - 0.0165590820x^3 + 0.8578371680x^2 - 23.9206488000x + 347.1731712001$	86.068
SAE-30	$y = 0.0006530445x^4 - 0.0792549324x^3 + 3.8266440679x^2 - 94.2916184083x + 1{,}124.1072250002$	211.331
SAE-15W-40	$y = 0.0007891542x^4 - 0.0949375833x^3 + 4.5423695833x^2 - 111.2240916667x + 1{,}328.0000000002$	242.094
10W-60	$y = 0.0006091667x^4 - 0.0765433333x^3 + 3.9208833333x^2 - 106.3096666667x + 1{,}453.8000000003$	319.955

Table 2.2: Dynamic Viscosity Calculated Values and Polynomial Trendline Regressions

2.2 Euler-Bernoulli Beam Vibration & Mode Shape

Once a method of determining viscosity at a given temperature was established, it was then time to derive the maximum displacement of the cantilever at any given point. The Euler-Bernoulli beam equation (eq 2.1) for undamped free vibration was used as a starting point.

$$EI\left(\frac{d^4(w(x,t))}{dx^4}\right) + \rho A\left(\frac{d^2(w(x,t))}{dt^2}\right) = 0 \qquad \text{Equation 2.1}$$

where:

- $w(x,t)$: displacement of cantilever at position (x) and at time(t)

- E: The elastic modulus
- I= Second moment of inertia $I = \left(\frac{b*h^3}{12}\right)$
- ρ=Density of the cantilever
- $A = Cross\ sectional\ area\ of\ the\ cantilever$

Of course, the cantilevers are not in an undamped, free vibrational state. A reasonable method was necessary to approximate (as close as possible) the real-world cantilever vibration scenario.

Given that the displacement of the cantilever depends on distance from the clamping position at a specific time for (eq 2.1), separation of variables is then needed to solve the Euler-Bernoulli partial differential equation for $w(x,t)$. In terms of separation of variables $w(x,t)$ equals the X(x) term multiplied by the T(t) term (eq 2.2), where $X(x)$ represents the mode shape of the cantilever and $T(t)$ representing the time domain.

$$w(x,t) = X(x)T(t) \qquad \text{Equation 2.2}$$

Generally, the mode shape equation is represented as (equation 2.3) below.

$$X(x) = A_n \cos(B_n x) + A_{n+1} \sin(B_n x) + A_{n+2} \cosh(B_n x) + A_{n+3} sinh(B_n x) \qquad \text{Equation 2.3}$$

where:

- X(x): Mode Shape
- x: Distance from clamping surface
- A_n: Undetermined Coefficients
- B_n: Beta Value for mode shape

The mode shape X(x) gives the unitless shape of the cantilever at any position along the cantilever.

2.3 Time Domain and Viscous Damping Model

It was necessary to determine a way of calculating the drag force on the tip of a cantilever immersed in a fluid before determining the time domain $T(t)$. The method that is Stokes-Law (eq 2.4).

$$F_D = 6\pi\eta R v \qquad \text{Equation 2.4}$$

The variable η represents the dynamic viscosity of the fluid flowing past the object in question. The variable v represents the velocity of the fluid with respect to the object in question. Stokes-Law's primary use is for drag force on a sphere through a fluid with given radius (R). However, Stokes-Law can be used to accurately estimate drag force on non-spherical objects. An equivalent radius for (R) is therefore determined. By equating the volume of the portion of the cantilever immersed in the fluid with the volume a sphere and solving for the radius equation (eq 2.5) was achieved.

$$R = \left(LWH\left(\frac{3}{4\pi}\right)\right)^{\frac{1}{3}} v \qquad \text{Equation 2.5}$$

Therefore equation (eq 2.4) then becomes (eq 2.6).

$$F_D = 6\pi\eta \left(LWH\left(\frac{3}{4\pi}\right)\right)^{\frac{1}{3}} v \qquad \text{Equation 2.6}$$

The remaining variables remain as previously defined.

Now that a method of relating the drag force due to a fluid of a certain relative velocity to dynamic viscosity has been determined it must now be integrated into the Euler-Bernoulli beam theory equation. For this a few assumptions have been made. For the real case, the sensor is a damped, forced vibration system. For the purposes of deriving an equation that will closely represent the real-world measured values it was beneficial to keep the equation as simple as possible and yet still maintain the necessary parameters. The first assumption made was that the

vibration of the system will be negligibly affected by the addition of the PZT-5H. This assumption was validated via a couple of different means. Given its mounting position high up on the cantilever, the piezo will not impart much of a moment of inertia due to its mass. The assumption was further verified once the natural frequency and displacement were calculated and compared to its measured value. The effects of viscous damping due to the air were also neglected given that its dynamic viscosity is nearly zero. It is also assumed that the real-world system could be closely approximated by modeling an undamped vibrating cantilever while accounting for the viscous damping term as a forcing function. The equation was therefore modeled as an undamped cantilever with the drag force on the cantilever represented as a forced vibration term. The Euler-Bernoulli equation. (eq 2.1) therefore becomes (eq 2.7) below.

$$\mathrm{EI}\left(\frac{\mathrm{d}^4(\mathrm{w(x,t)})}{\mathrm{dx}^4}\right) + \rho\mathrm{A}\left(\frac{\mathrm{d}^2(\mathrm{w(x,t)})}{\mathrm{dt}^2}\right) + \mathrm{G}\left(\frac{(\mathrm{w(x,t)})}{\mathrm{dt}}\right) = 0 \qquad \text{Equation 2.7}$$

The third (rightmost) term in (eq 2.7) represents the drag force on the tip of the cantilever determined by (eq 2.6)

where:

- $G: 6 * \pi * \eta * \left(L * W * H * \left(\frac{3}{4\pi}\right)\right)^{\frac{1}{3}}$
- $\left(\frac{d(w(x,t))}{dt}\right)$: The change in position with respect to time

As the cantilever vibrates back and forth in the tested fluid, it will increase and decrease in velocity as it oscillates. Thus, the “Stokes-Law” equation must include a velocity term that is a derivative of the cantilever displacement with respect to time and distance from clamping position. After implementing the method of separation of variables resulted in (eq 2.8).

$$\frac{(E*I)}{\rho*A}\left(\frac{X(x)^{IIII}}{X(x)}\right) = \left(\frac{(T(t)^{"})}{T(t)}\right) + \left(\frac{F}{\rho*A}\right)\left(\frac{T(t)'}{T(t)}\right) = -\omega^2 \qquad \text{Equation 2.8}$$

Solving the Euler-Bernoulli beam equation now in terms of separation of variables for the time domain T(t) yields (eq 2.9).

$$T(t) = e^{-Nt}(C_1 cos\left(\sqrt{(N^2 - \omega^2)t}\right) + C_2 cos\left(\sqrt{(N^2 - \omega^2)t}\right)) \quad \text{Equation 2.9}$$

where:

- T(t): Time Domain where "t" is time is seconds.
- ω: The natural frequency of the Cantilever
- C_1, C_2: Undetermined Coefficients
- N: $\left(\frac{\left(3\pi\eta\left(LWH\left(\frac{3}{4\pi}\right)\right)^{\frac{1}{3}}\right)}{\rho * A}\right)$

As the maximum value of the time domain is the only value of interest, the value of "t" can be treated as an unknown constant value. Furthermore, as there were no initial conditions available for the time domain there is no practical way to derive an exact solution the time domain as C_1 and C_2 could not be calculated. Therefore, the term $(C_1 cos\left(\sqrt{(N^2 - \omega^2)t}\right) + C_2 cos\left(\sqrt{(N^2 - \omega^2)t}\right))$ of (eq 2.9) can now be collapsed into the unknown constant coefficient "K". As for the e^{-Nt} term of (eq 2.9), the "t" value will be represented as another unknown constant "Q". The final equation for the time domain (eq 2.9) therefore becomes (eq 2.9).

$$T(t) = Ke^{(-QN)} \quad \text{Equation 2.9}$$

By inserting (eq 2.3) and (eq 2.9) into (eq 2.2) results in (eq 2.10).

$$w(x,t) = A_n cos(B_n x) + A_{n+1} sin(B_n x) + A_{n+2} cosh(B_n x) + A_{n+3} sinh(B_n x)\left(Ke^{(-QN)}\right) \quad \text{Equation 2.10}$$

The unknown constants “Q” and “K” can be derived for with the experimental results (section 4.5). The unknown constants “Q” and “K” are now regarded as calibration coefficients for the raw data. Given that the unknown constant K will be experimentally attained it was not necessary to derive a value for the actual mode shape as this will be a constant as well. Therefore, the mode shape was absorbed into the “K” constant of (eq 2.10) giving the final equation as (eq 2.11) below.

$$w(x,t) = Ke^{\left(-Q\left(\frac{\left(3\pi\eta\left(LWH\left(\frac{3}{4\pi}\right)\right)^{\frac{1}{3}}\right)}{\rho * A}\right)\right)} \qquad \text{Equation 2.11}$$

This doesn’t invalidate the theoretical results. The important part of the theoretical calculations is the relative correlation between the dynamic viscosity “η" and the displacement $w(x,t)$.

CHAPTER 3

FINITE ELEMENT MODELING

Before beginning any experimentation, it was necessary to determine the first mode resonant frequency for each cantilever. Finite element analysis (FEA) was performed using ComSol to ascertain an estimate for the natural frequency for each cantilever while undergoing no effects due to viscous drag. Once found, this information made it much easier to find the first mode resonant frequency experimentally. The resonant frequency during actual experimentation with tip immersed will be below the values attained under FEA simulation due to the effects of viscous damping. The material parameters that were considered in the FEA simulation for all 3 cantilevers are as below (Table 3.1).

Parameter	Cantilever Value	Piezo Value
Material Name	301 (UNS S30100)(SUS 301)[average]	Lead Zirconat Titrate (PZT-5H)
Density (kg/m^3)	8050	7500
Young's Modulus (Pa)	1.93E+11	6.30E+10
Poison's Ratio (nu)	nu(T[1/K])	0.31

Table 3.1: FEA Material Parameters

The piezo was attached to the cantilever in via the “Union” function under the Geometry dropdown within the ComSol model builder pane. As the FEA needs to simulate “fixed-free” cantilever boundary conditions it was necessary to account for the fixed constraint. The end of the cantilever closest to the piezo (seen in (Fig 3.2.-3.4.) as the upper left thin edge of the cantilever) was fixed in place to simulate the clamping condition of the physical experiment. This was done using the “Fixed Constraint” tool under the “Solid Mechanics” dropdown on the model builder pane.

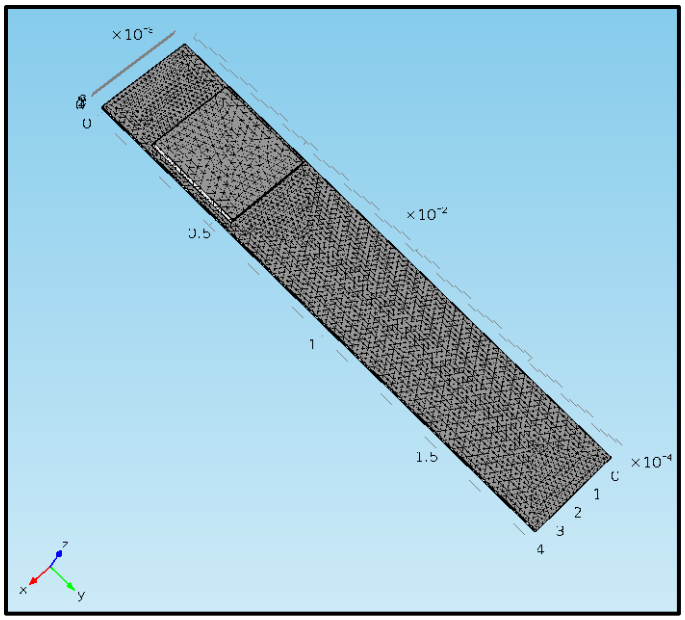

Figure 3.1: Mesh Density Sample (Zero-Step)

(Fig 3.1.) is an example of the automatic mesh calculation performed within ComSol set to “normal” under the “Element Size” dropdown within the mesh tool on the model builder pane. An “Eigenfrequency” study was performed to attain the resonant frequency. No accommodations for effects due to air were performed as they were negligible. (Figures 3.3.-3.5.) display the graphical representation of the cantilevers under max deflection during the first frequency mode.

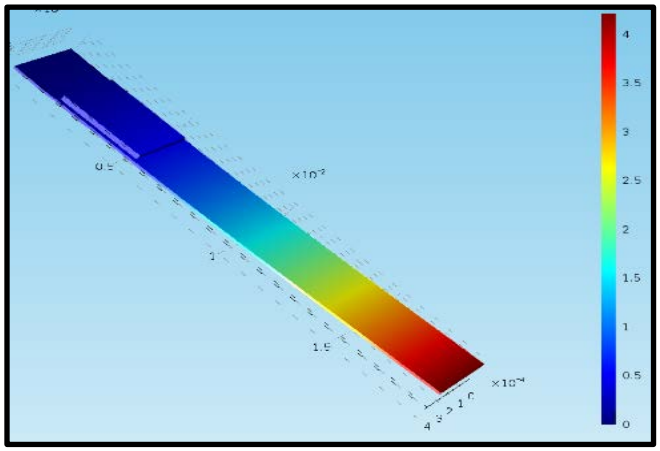

Figure 3.2: Zero-Step Cantilever-ComSol

Eigenfrequency Mode (Hertz)	Zero-Step
1st Mode	278.86
2nd Mode	1342.6
3rd Mode	2718.5
4th Mode	3770.3
5th Mode	7522.9
6th Mode	8212.2

Table 3.2: Zero-Step First 6 Eigenfrequencies

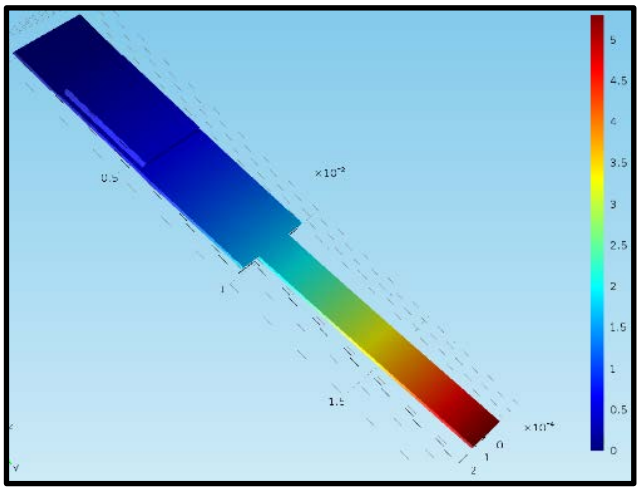

Figure 3.3: One-Step Cantilever-ComSol

Eigenfrequency Mode (Hertz)	One-Step
1st Mode	332.61
2nd Mode	1207.1
3rd Mode	3468.6
4th Mode	4905.8
5th Mode	7210.4
6th Mode	8033.6

Table 3.3: One-Step First 6 Eigenfrequencies

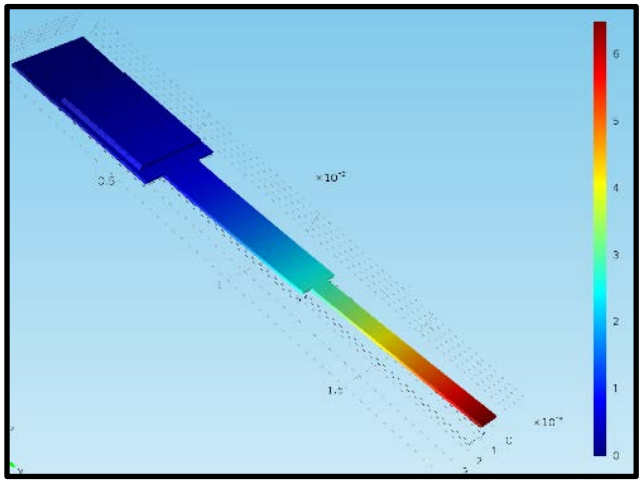

Figure 3.4: Two-Step Cantilever-ComSol

Eigenfrequency Mode (Hertz)	Two-Step
1st Mode	394.3
2nd Mode	1288.9
3rd Mode	3131.3
4th Mode	7228.8
5th Mode	7438.1
6th Mode	7949.2

Table 3.4: Two-Step First 6 Eigenfrequencies

Each cantilever of (Fig 3.3-3.5) represents deflection magnitude chromatically. The chromatic scale itself (on the rightmost side of each figure (Fig 3.3-3.5) represents deflection in relative terms and do not correspond to any actual displacement unit. The values of (Table 3.2-3.4.) are output by ComSol are in units of Hertz (HZ). The “Eigenfrequency” study within ComSol was set to output the first 6 natural eigenfrequency modes (Table 3.2-3.4). For the purposes of experimentation only the 1st Mode frequencies were considered.

CHAPTER 4

EXPERIMENTAL ANALYSIS

4.1 Cantilever Viscometer Fabrication

The three cantilevers were fabricated from a 0.1mm thick sheet of stainless-steel. The stainless-steel sheet was initially cut into a circle roughly the same diameter as the mold used to set it in acrylic. The stainless-steel sample was then placed at the bottom of the circular mold. Liquid two-part acrylic resin was then poured on top of the stainless-steel sample and allowed to cure. Once cured the sample was removed from the mold. A DXF file was then created for the desired shapes of the cantilevers to be cut out of the stainless-steel sample. The acrylic sample with imbedded sample was then cut on a CNC laser cutting machine guided by the DXF file. (Figure 4.1) shows the sample after the laser cutting process

Figure 4.1: Acrylic Sample Post Laser Cutting

The piezo started life as an American-Piezo brand PZT-5h that was 10 X 10mm and 0.5mm thick. The experiment necessitated that the piezo be ground down to a 0.2mm thickness. To accomplish this the PZT-5h was first mounted in acrylic in the same fashion as the stainless-steel used to make the cantilevers.

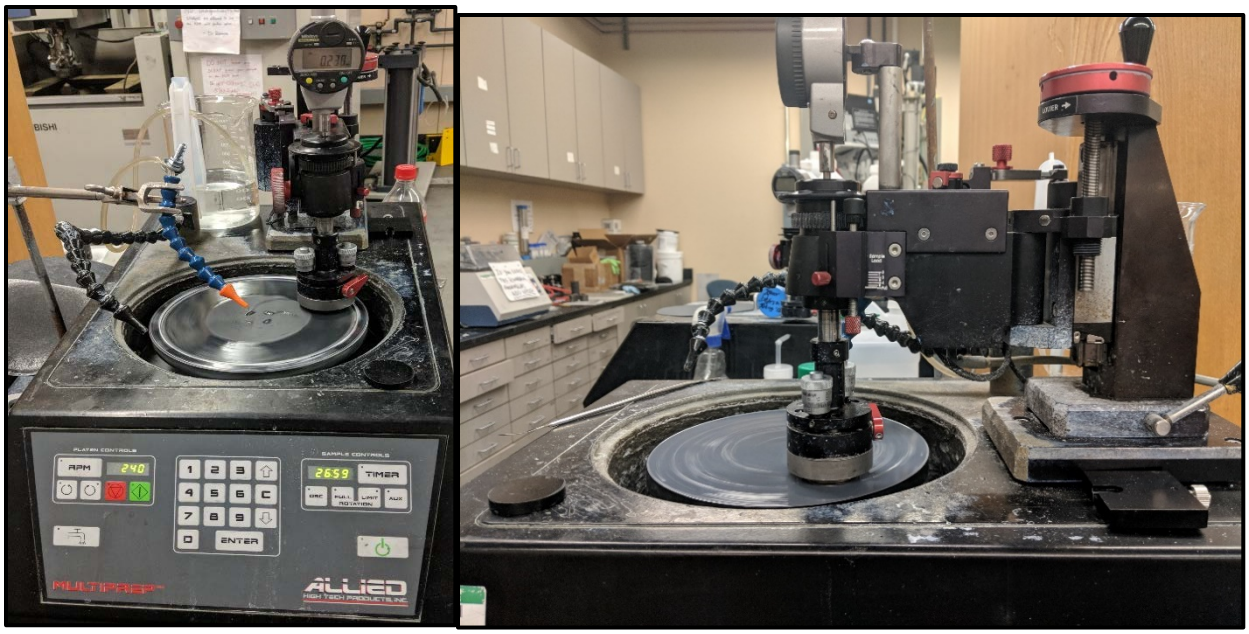

Figure 4.2: Automatic Sample Polisher/Grinder

An automatic sample polisher/grinder (Fig 4.2.) was used to grind the sample to the desired thickness. The piezo side of the sample was first mounted face up in the grinder as to flatten and level the opposing side of the sample to make the two circular sides coplanar. The sample was then mounted piezo-side down against the grinding surface and progressively ground until the desired until 0.3mm had been removed.

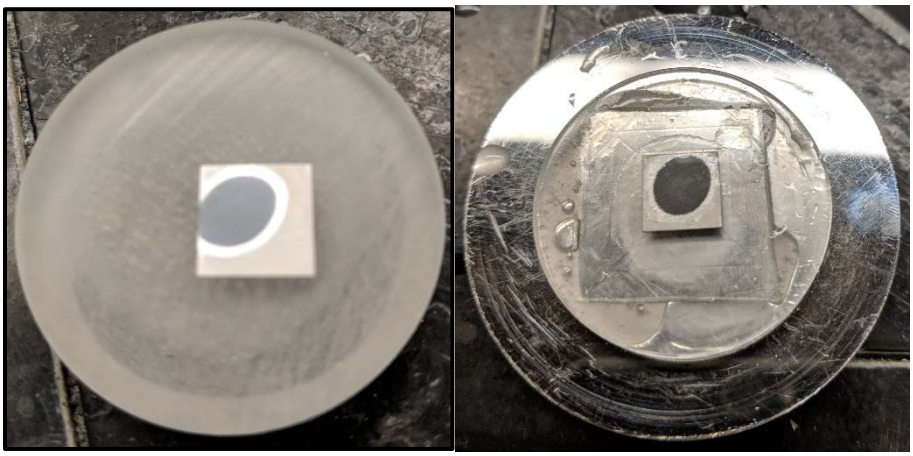

Figure 4.3: Piezo Acrylic Sample (Polishing)

Once ground and polished (Fig 4.3.), it was necessary to replace the electrode ground off during the thinning of the piezo. This was achieved via Electron Beam Evaporation [24] at the universities cleanroom.

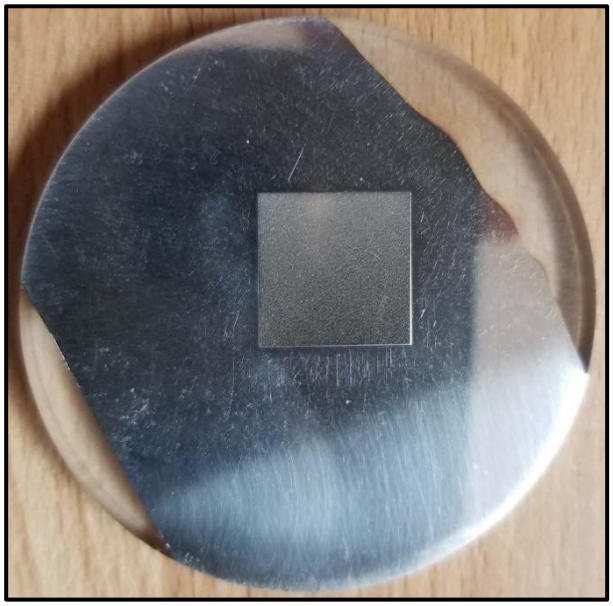

Figure 4.4: Acrylic Sample (Post Electron Beam Evaporation)

The PZT-5h was then cut into 4 X 4mm squares using the same CNC laser cutting process used to cut the cantilevers. After the cutting process the acrylic was left attached to the square piezos that were cut out of the larger sample (Fig 4.5). The reason for this is discussed in the subsequent paragraph.

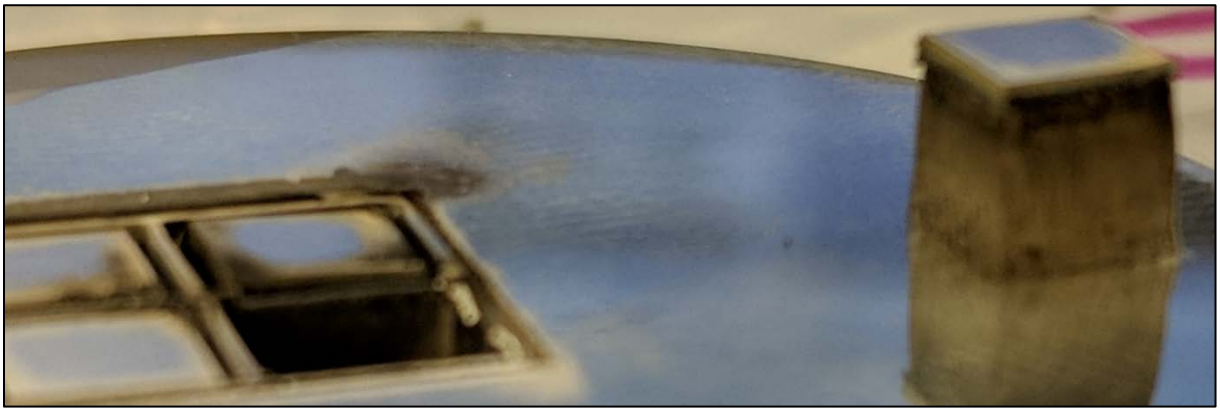

Figure 4.5: Acrylic mounted PZT-5H (Post Laser Cutting)

The piezo then had to be mounted to the cantilevers. However, the placement of the piezos first had to be marked on the cantilevers themselves. As the distance for each piezo position from the clamping-end edge was the same for all three cantilevers, their reference line could be made at the same time. This reference line was positioned using the widest step on the two-step cantilever as a reference. As this step corresponds to one edge of the piezo for this cantilever it made a convenient reference for all three. This is however assuming the short edge of the clamping ends of each cantilever were aligned to each other. To achieve the consistent placement of the reference-line on each of the cantilevers required a bit of ingenuity. A scrap piece of plastic was used as the base for mounting the cantilevers for marking. A section of wide scotch brand blue painters tape was placed sticky-side up on the plastic base. The edges of this tape were themselves taped down to the plastic base. A scrap piece of the 0.1mm stainless steel (cut from the edge of the sheet for a perfect straight edge) was then placed on the edge of the sticky section of the tape. The straight edge of the stainless steel being used as a datum line to align the cantilevers with each other. All three of the cantilevers were placed parallel to each other on the sticky-side up tape with long edges touching. Assuring the clamping end of each cantilever was perpendicular and butting up against the datum the cantilevers were then aligned to each other. Cutting two pieces of tape the same length as the distance between the first shoulder of the two-step cantilever and the clamping-end edge gave two reference points by which to align the reference line for placement of the piezo. These pieces of tape were placed adjacent to the long edges of the outer two cantilevers, making sure to align them with the datum as well. A piece of tape was then placed on the opposite ends of the pieces of reference tape across all three piezos to create the reference line for placement of the piezos.

Now that an accurate reference line had been placed, it was now time to mount the piezos

themselves. This was a very involved task in and of itself requiring a fair amount of dexterity. The piezos are very small at only 4X4mm as well as 0.2mm thick which is thinner than the manufacturers recommendation. Due to the 0.2 mm thickness the piezos they were extremely delicate and were easily broken if care wasn't employed to prevent damage. Therefore, the acrylic was left attached to each 4X4mm piezo for support during the bonding process to the cantilevers (Fig 4.5.). The piezos needed to lay flat on the cantilever to ensure that the piezo driving force was perpendicular to the "width-length" plane of the cantilever. The bonding method as a consequence had to be electrically conductive. Electrically conductive (WireGlue Brand) glue facilitated the conduction of electricity from each cantilever to its piezo. However, this glue was not up to the task of ensuring a strong bond between the piezos and cantilevers on its own. To further the difficulty of bonding the piezos to their cantilevers, a a two-part (3M brand) epoxy had to also be used. Before laying down any glue, the cantilevers were first sanded with 180 grit sandpaper. The surfaces were then prepped using isopropyl alcohol to remove any contaminants. The mounting of the piezos was done individually due to the short working time of each glue. As the cantilevers were right next to each other the adjacent cantilevers to the one currently being bonded were covered with yet another piece of blue painter's tape to prevent any excess glue from settling on the bonding surfaces prior to moving on to them.

Applying the glue to the cantilevers was a bit of a "trial and error" process and extremely tricky. The "working time" of the electrically conductive glue was somewhat shorter than the two-part epoxy, roughly 45 seconds. The two-part epoxy after mixing had a useful working time of about 2 minutes or so. That is not to say the curing time was 45 seconds, it simply was too dried out after that time to ensure electrical conductivity as well as mounting the piezo flat on the cantilever. Yet another added difficulty was the glue tended to separate after only a couple

minutes with the iron filings settling to the bottom, requiring thorough mixing. Therefore, it was pertinent to establish an "order of operations" to the process.

4.2 Bonding Process

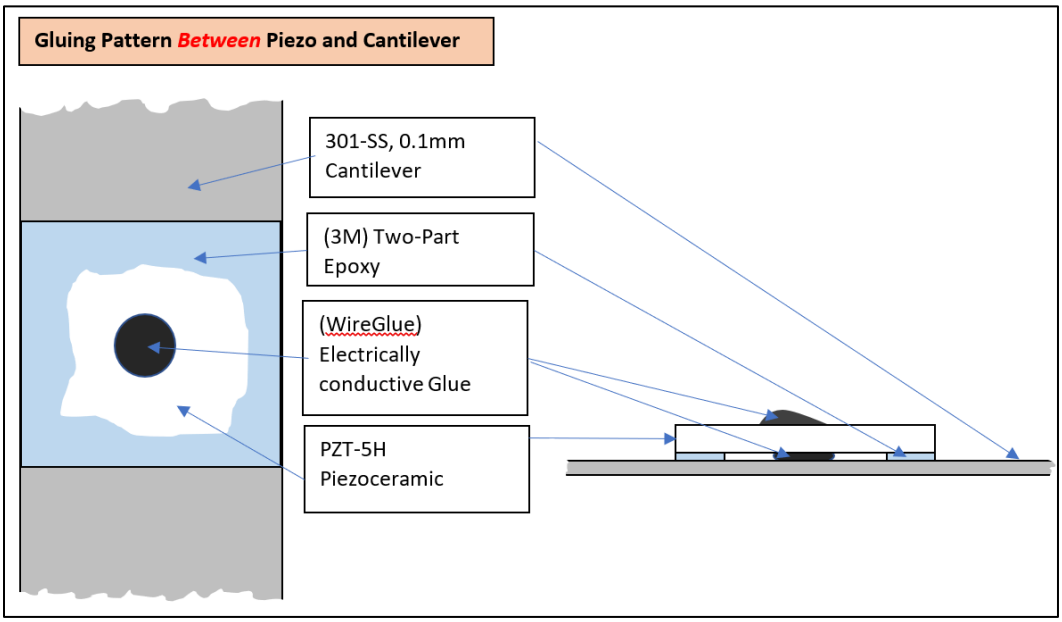

Figure 4.6: Cantilever-Piezo Gluing Pattern Reference

1. A wooden coffee stirring stick (like a popsicle stick except longer and thinner) was cut it in half using a diagonal cut. The diagonal cut should be approximately 1 inch long along its hypotenuse. A single strand of 20-gauge stranded wire was also required.
2. Pre-mix the electrically conductive glue to reduce the mixing time required later.
3. A "marble sized" amount of two-part epoxy was deposited onto a mixing surface. Using any less than this amount would greatly increase the chance of not having equal amount of each part of the epoxy resulting in it not curing. Using another coffee stirring stick the epoxy was mixed thoroughly for about a minute. There was now only about two minutes to accomplish the following steps.

4. The electrically conductive glue was further mixed for about 30 seconds. Using the single strand of braided wire to deposit the electrically conductive glue, a very minimal amount was placed at the center of the square section of the cantilever surface where the piezo will be placed. Using the wire move the glue around until a roughly 1mm diameter circle of glue was covering the center of the mounting surface (Fig 4.6.).

5. Using the pointed end of the diagonally cut wooden mixing stick, a very thin layer of glue was applied to the mounting surface around the conductive glue (Fig 4.6.).

6. The piezo was then placed onto the cantilever with the aid of a pair of tweezers grabbing onto the acrylic backing. It was imperative not to move the piezo around once in in contact with the glues to prevent them mixing as this would prevent electrical conduction. The piezo also tended to float around on top of the glue. It therefore had to be held into place for few minutes with tape to prevent it from moving out of position while the glue sets up.

Once the bond had been allowed to cure for about 8 hours (per manufacturer recommendations for the two-part epoxy) the acrylic piezo backing had to be removed. This was done by immersing the entire cantilever in acetone to dissolve off the acrylic. A single strand of 20-gauge stranded wire was then attached to the now exposed electrode of the piezo using a minimal dot of electrically conductive glue at the center of the electrode. This process was repeated for all three cantilevers.

4.3 Cantilever Viscometer Fabrication (Amended)

Section 4.1 describes the initial cantilever fabrication used during the initial experimentation. This section describes the amended methods that were necessary for completion of the experiments. The fabrication method was changed due to a myriad if reasons.

This section covers the amended cantilever fabrication process ultimately used for the results in this experimental research. The original AmericanPiezo brand PZT-5H piezos that were fabricated were unsalvageable. Therefore, a Boston Piezo Optics Inc. brand PZT-5H was acquired, already at the desired 0.2mm thickness.

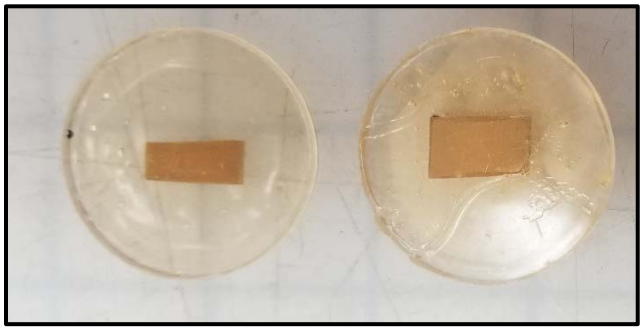

Figure 4.7: New Piezo Acrylic Samples Boston Piezo Optics Inc. [33]

Figure 4.8: Jewelers Saw [32]

The new piezo was again mounted in acrylic to support it during the cutting process (Fig 4.7.). A new method was employed for cutting of the 4x4x0.2mm piezos required for experimentation. The amended cutting method used for fabrication of the final viscometers ended up being a jewelers saw as pictured in (Fig 4.8.). This method was far superior to the CNC laser method as it reduced the risk of depolarizing the edges of the piezo due to the heat of the CNC laser as well as the ability to accurately (requiring some skill) cut it to the desired dimensions.

4.4 Bonding Process (Amended)

The reliability and repeatability of the initial cantilever was severely lacking. It proved quite difficult to repeat the experimental results from what day to the next. Furthermore, the piezo on the Two-Step cantilever fell off during an experimental run. Both problems were symptoms of improper bonding between the piezo and the cantilever. The two-part epoxy had

not hardened properly causing inconsistent results as well as bonding issues. Furthermore, due to the soft epoxy between the piezo and the cantilever, there was poor propagation of the oscillation force of the piezo to the cantilever. A major reason for this was due to the acetone used to remove the acrylic backing from the back of the piezo. The acetone had softened the two-part epoxy. Therefore, the acrylic on the piezos used for this new method was removed first before bonding it to the cantilever. As before, a single strand of wire was bonded to the top of the piezo using the electrically conductive glue. The electrically conductive glue had the added benefit of acting like a backing material to support the piezo during bonding. The attached wire also helped to position the piezo during bonding.

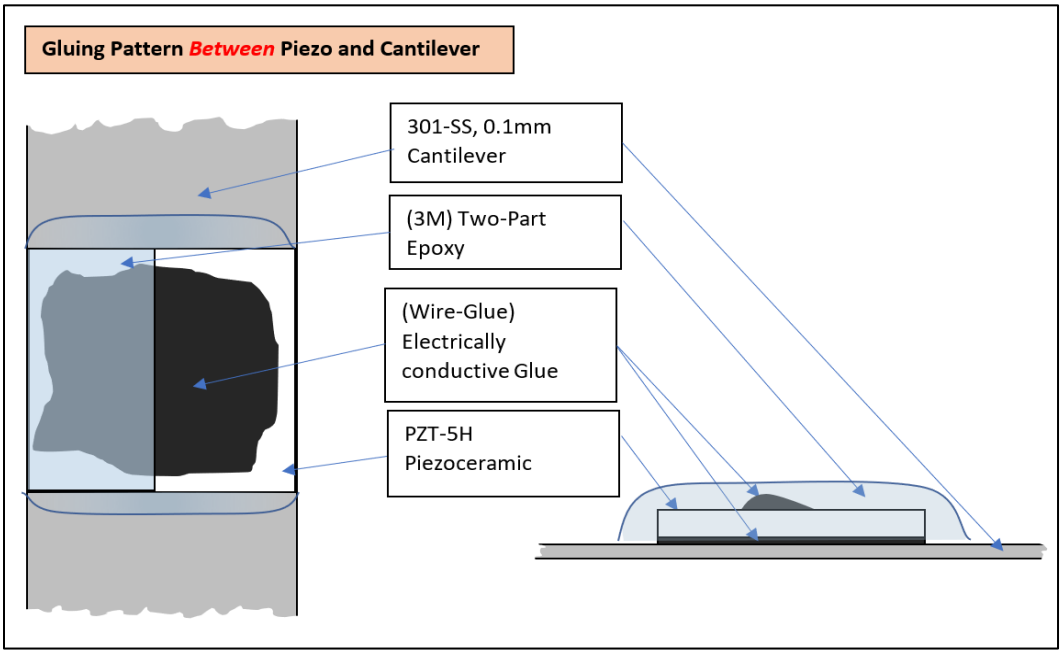

Figure 4.9: Cantilever-Piezo Gluing Diagram (Amended) [32]

The new bonding process (detailed in (Fig 4.9.)) uses the electrically conductive glue only between the piezo and the cantilever. A cap of two-part epoxy was added on top of the piezo and cantilever for additional strength (Fig 4.9.).

4.5 Test Bed Description

This section describes the actual equipment and methods used to set up the experiment. The clamping methodology, measurement equipment, as well as all associated equipment is discussed in detail.

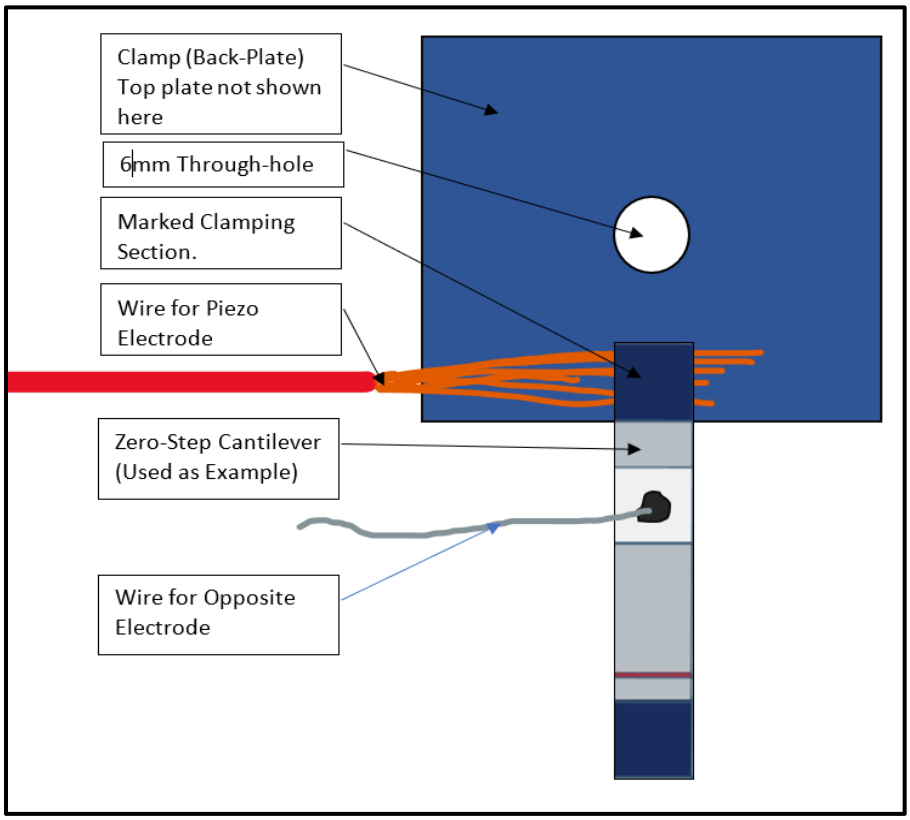

Figure 4.10: Clamped Cantilever Electrical Configuration Reference Diagram

Firstly, a method of mounting the cantilever viscometer under a clamped-free boundary condition was devised. A passive vibration isolation scientific table was used to set up the experiment. A clamp was then fabricated using 3/8” aluminum plate. The plate was cut into two ~1.5” square sections. A 6mm hole was then drilled through both square aluminum sections and a bolt was passed through to allow for mounting as well as tighten the clamp (Fig 4.11.-4.12.).

The interior mating surfaces of the clamp were insulated using simple blue painters tape. The insulation was to prevent any electricity traveling to the stainless steel worksurface of the

scientific table and adversely affecting the electric signal. A stranded 20-gauge wire (Red wire of (Fig 4.4)) was inserted between the mating surfaces of the clamp to conduct the electric signal through to the cantilever viscometer. When mounting the cantilever in the clamp, it was pertinent to make sure to align the cantilever's clamping section with the bottom edge of the (Fig 4.11.-4.12.). The electrical continuity between the cantilever and the red 20-gauge wire was then verified with a multimeter. Two vertical extruded aluminum supports were bolted to the surface of the scientific table. An extruded aluminum crossmember was then bolted between the vertical supports creating a gantry. The clamp along with cantilever viscometer was then bolted to this crossmember (Fig 4.11.-4.12.).

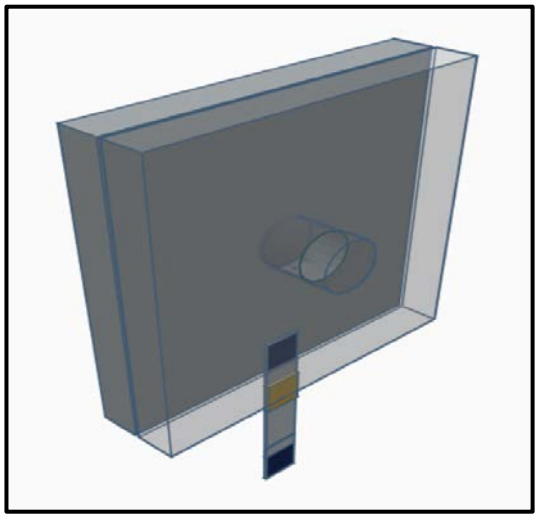

Figure 4.11: Clamp CAD Diagram

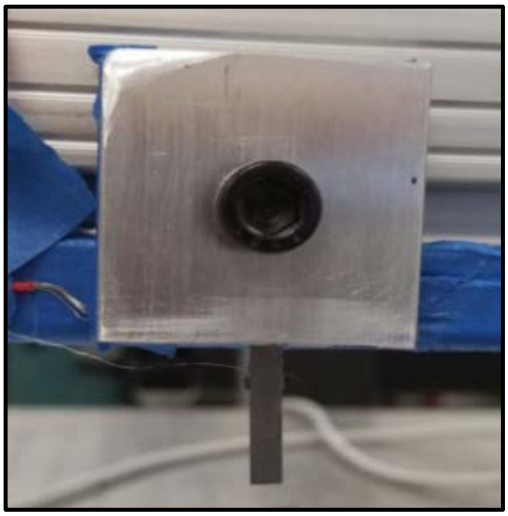

Figure 4.12: Cantilever Clamp

Next, a method of accurately setting the immersion depth of the tip of the cantilever into the testing fluid was necessary to conduct the experiment. An adjustable platform jack was 3d printed as seen in (Fig 4.14.-4.15.) as the black plastic device under the cantilever/clamp. A spring was installed onto the platform jack's scissor mechanism to take up the slack in the mechanism to further facilitate accurate setting of the immersion depth.

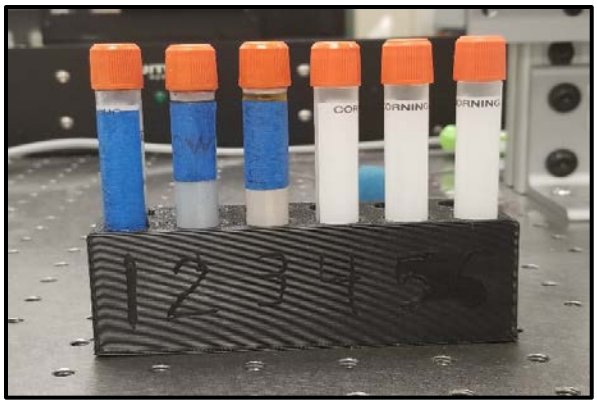

Figure 4.13: Test Tubes Containing Testing Samples

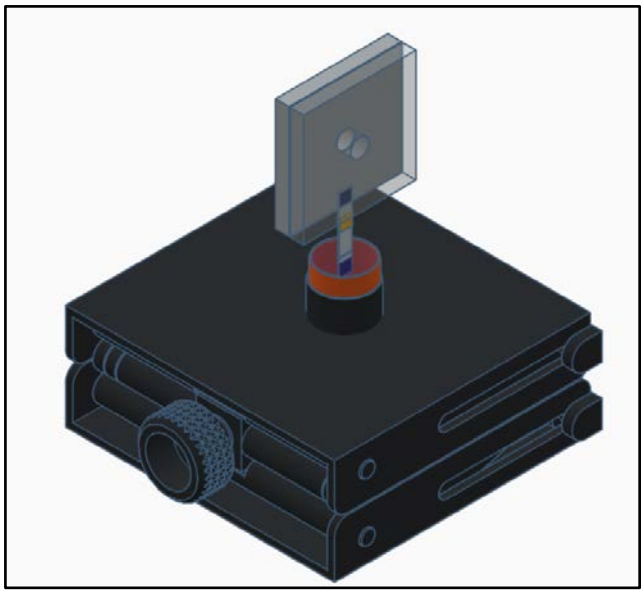

Figure 4.14: Clamp, Viscometer, and Platform Jack CAD Representation

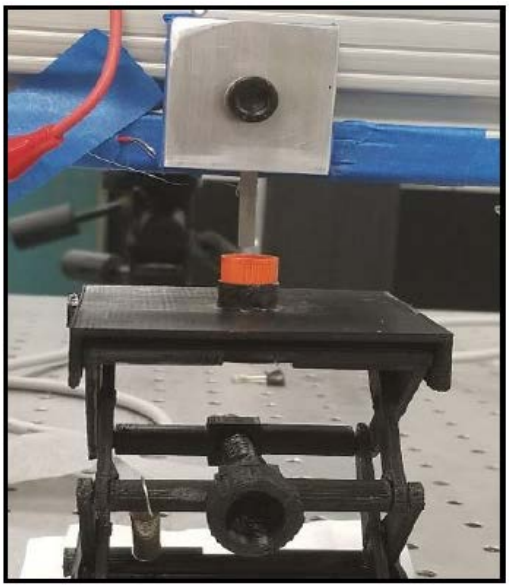

Figure 4.15: Clamp, Viscometer, and Platform Jack

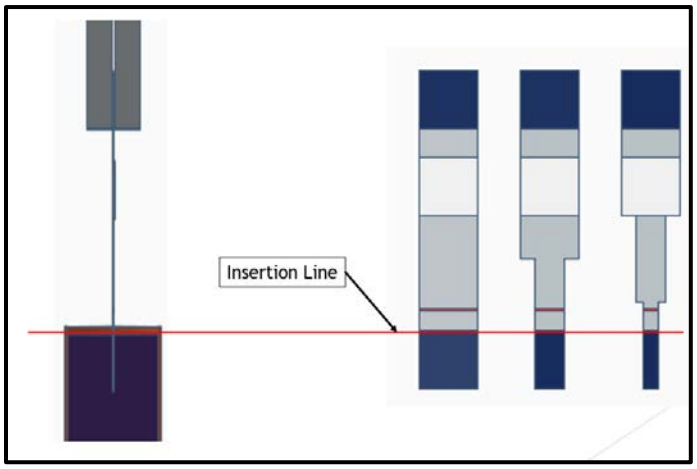

Figure 4.16: Laser Alignment Reference Diagram

Each fluid testing sample was placed in plastic test tubes with a screw-on sealed orange cap (Fig 4.13.-4.15.). It is worth noting that the level of oil (testing fluid) in each test tube were equal in each and stored relatively close to each other (Fig 4.13.) for a good reason. This was done in an attempt to make sure that each testing sample remained the same temperature with reference to each other as the room temperature varied. The orange cap of the test tubes conveniently doubled as the testing fluid reservoir. A circular socket was acetone-welded to the top of the platform jack to firmly hold the test tube cap in a fixed position under the cantilever as seen in (Fig 4.14.-4.15.). The laser beam itself was aligned per (Fig 4.16.) for all 3 cantilevers.

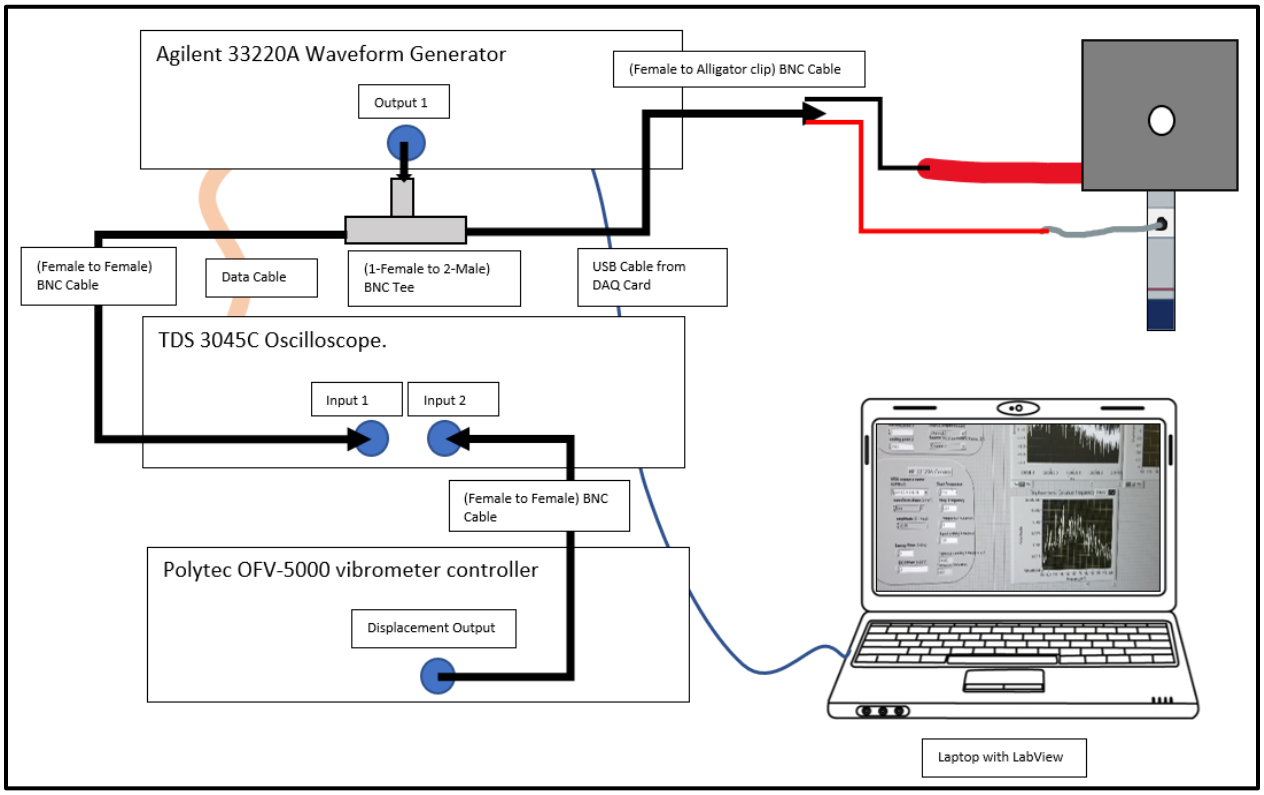

Figure 4.17: Equipment Block Diagram

A female BNC cable equipped with alligator clips was affixed to the 20-gauge red wire as well as the wire attached to the exposed surface of the viscometer's piezo. The female end of this BNC cable was then attached to the Agilent 33220A Waveform Generator through a T-

splitter (Fig 4.18. (Top)). The waveform generator was then able to supply the electrical signal to the piezo. A female to female BNC cable was then attached to that same T-splitter with the other end going to input-1 of the Tektronix TDS-3054C Oscilloscope. This allowed for monitoring of the waveform generator signal being sent to the viscometer as seen in (Fig 4.21.) as the top yellow sinusoidal signal.

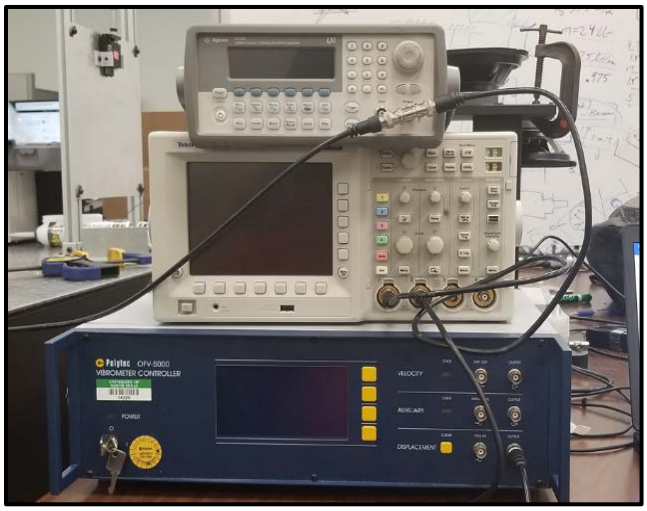

Figure 4.18: Measurement Equipment Reference Picture

The Polytec OFV-505 laser vibrometer (Fig 4.19.) actively measure the cantilever viscometers displacement during oscillation. A Polytec OFV-5000 vibrometer controller (Fig 4.20., Fig 4.18. (Bottom)) running the DD-900 displacement decoder software. A second female to female BNC cable was connected from the vibrometer controller's displacement output to input-2 of the oscilloscope (Fig 4.18. (Middle))

Figure 4.19: OFV-505 Laser Vibrometer [21]

Figure 4.20: OFV-5000 Vibrometer Controller [22]

Under the vibrometer controller menu the displacement setting was selected. Within the displacement setting the most appropriate range for the output signal from the vibrometer controller. The selection of this range was chosen based on what gave the most consistent resonant amplitude between runs for a specific testing fluid.

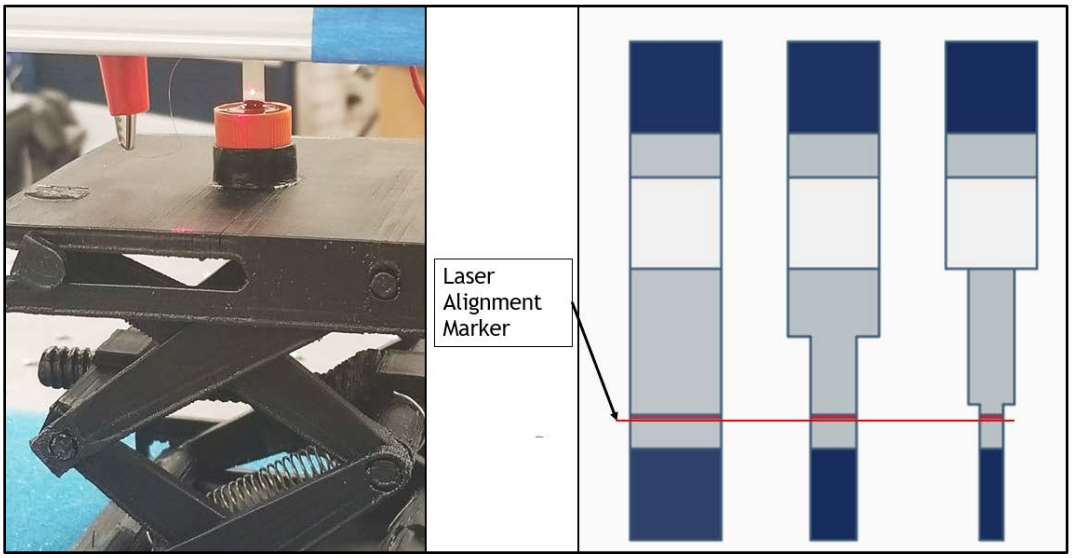

Figure 4.21: Laser Vibrometer Alignment Picture and Reference Diagram

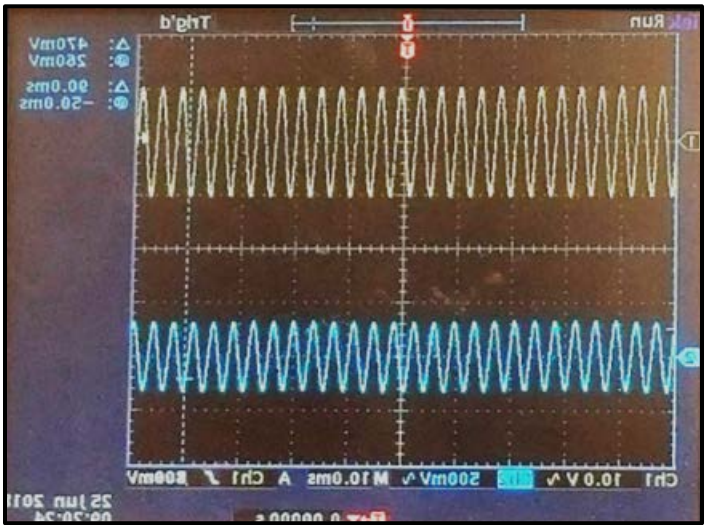

Figure 4.22: Sample Oscilloscope Waveforms

The vibration of the cantilever as measured by the laser vibrometer could then be monitored on the oscilloscope as seen in (Fig 4.21.) as the bottom blue sinusoidal signal.

4.6 Test Bed Description (Amended)

(Fig 4.22.) was the final configuration of the cantilever clamp. The original method was dropped due to inconsistent electrical continuity.

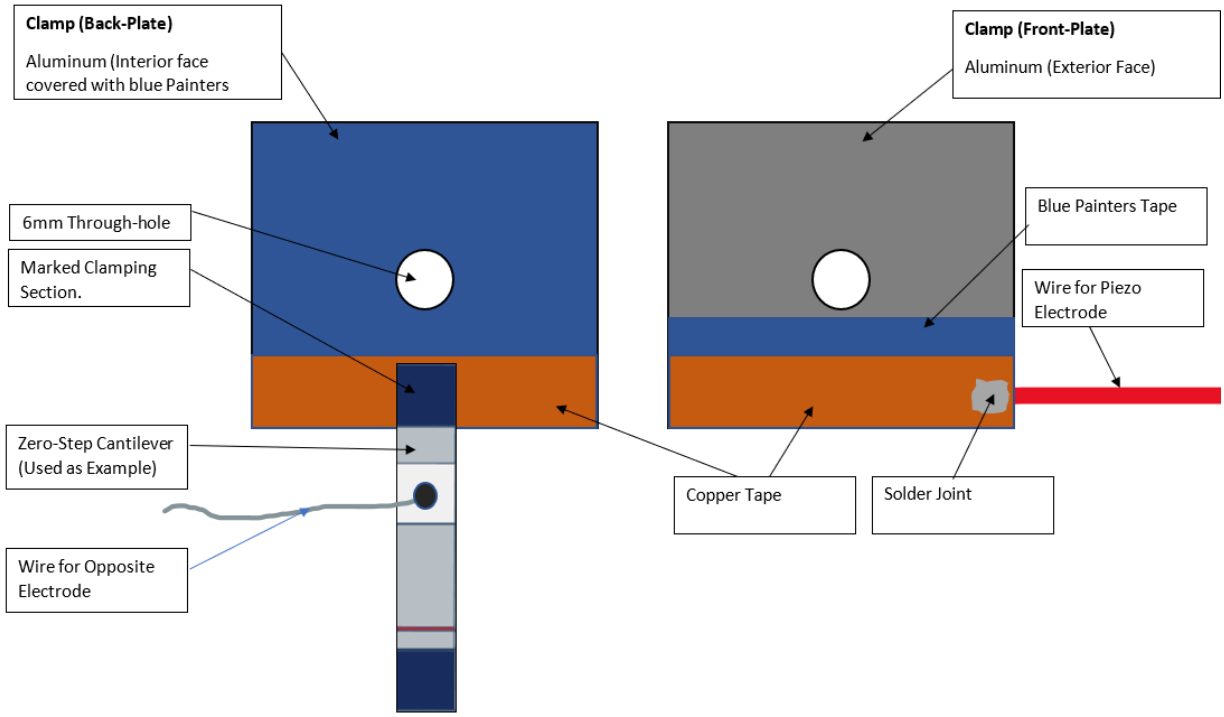

Figure 4.23: Clamped Cantilever Electrical Configuration Reference Diagram (Amended)

The interior faces of the cantilever clamp were covered in copper tape as pictured in (Fig 4.2.2.). The red wire was soldered to the top face of the outer clamp. Before application of the copper tape, 2 layers of blue painter's tape were put on both sides on the interior faces of the clamp.

4.7 Sweep Testing

Using the undamped 1st mode resonant frequencies acquired from the ComSol FEA as a starting point, the resonant frequency viscometer with tip immersed in the testing fluid could be easily approximated. The immersed resonant frequency was attained by manually decreasing the

signal frequency from the waveform generator until the signal from the vibrometer ((Fig 4.21). (bottom blue signal)) reached peak amplitude. Next an appropriate range for the frequency sweep was attained where the resonant frequency was approximately the midpoint of that range. The minimum range for the sweeping frequency was determined to be a minimum of 100Hz. This 100Hz minimum range was based on providing a wide enough graph for accurate trendline fitting. A LabView program LabView was used to record the amplitude of the vibrometer sinusoidal signal during each frequency step over the selected range of frequencies. The settings for the LabView program are listed in (Table 4.1.).

Parameter	
Sweep Time (Seconds)	1
Waveform Shape	Sine
Amplitude (V_pp)	20
DC Offset (V)	0
Input waiting time (ms)	500
Source_function Generator	Channel 1
Source_Displacement	Channel 2
Starting Point 2	0
Ending Point	2000

Table 4.1: LabView Input Parameters

LabView, once finished with the sweep, would then display a plot of its readings such as in (Fig 4.24.). The LabView data table used to make the plot (Table 4.1) was then exported to Microsoft Excel to be further analyzed. Each measurement was run four times during the testing of each viscosity the purposes of further experimental control. The experimental redundancy eliminates the chance of an errant or “fluke” reading.

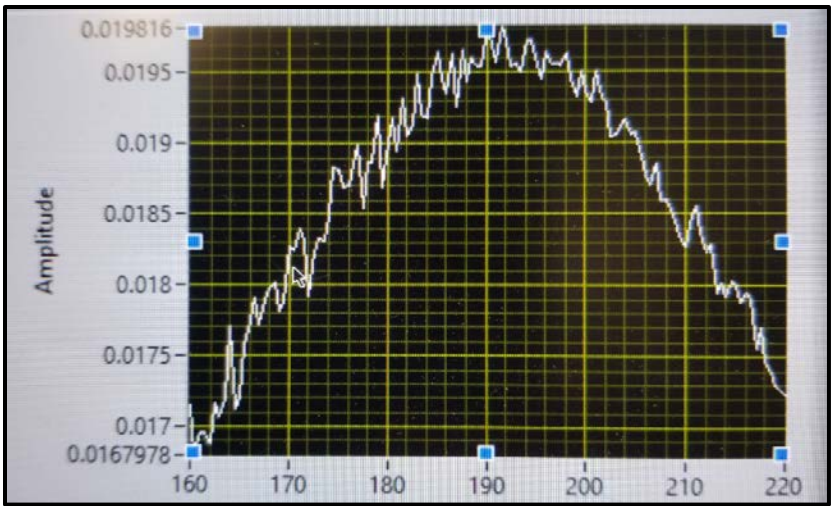

Figure 4.24: Sample LabView Displacement Graph

4.8 Experimental Results

The intent of the experimentation was to analyze each of the three microcantilever viscometers under five different operating parameters.

- Atmospheric Air (Fully immersed)
- SAE-5W-20 (4mm Tip insertion)
- SAE-30 (4mm Tip insertion)
- SAE-15W-40 (4mm Tip insertion)
- SAE-10W-60 (4mm Tip insertion)

All tests were performed with the testing fluid at 23 Celsius. For each operating condition, four experimental runs were performed. The range of the laser vibrometer displacement setting was set to 5 micrometers per volt (um/v) for all runs for each operating parameter. (5um/v) was chosen through “trial and error” based on the minimum setting which gave consistent resonant amplitude values between trials. As stated previously, the laser vibrometer was aimed at position (x=12mm) along the cantilever, as measured from clamp face.

The experimental results for all tests were analyzed using Microsoft Excel. The first step in this process was to graph the table of frequency steps and corresponding amplitude values that have been exported from LabView. A scatter plot was made of the average of the four runs for each of the tested oil samples (operating conditions). (Fig 4.25.) is an example of the averaged voltage amplitude values (y-axis) from the Two-Step vibrometer for SAE-5W-20 over the frequency sweep range (x-axis).

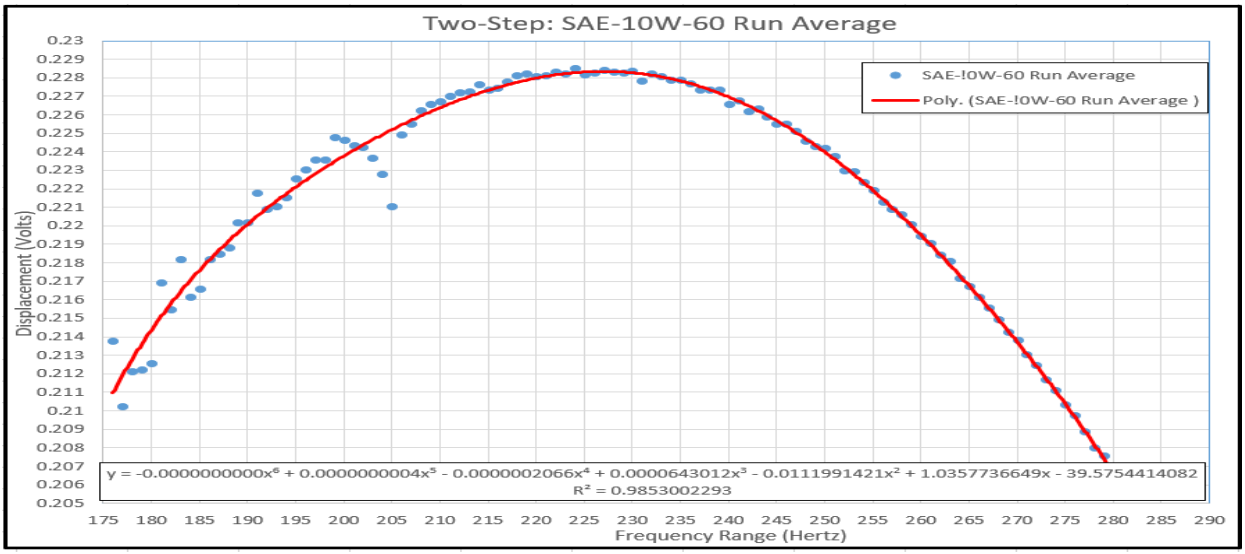

Figure 4.25: Sample Excel Trendline Fitting to Averaged LabView Exported Data Set

A trendline is then fitted to the scatter plot values using a sixth order polynomial-type trendline. A polynomial was chosen because upon inspection of the scatter plot points (Fig 4.25. (blue dots)), it seems to follow a polynomial-type curve. (Fig 4.25. (red line)) shows an example of the trendline fitting that was performed in Microsoft Excel. Next, an equation was automatically generated via Excel for the polynomial trendline. It is worth noting that the numerical values within the trendline were taken to 20 decimal points to assure adequate accuracy. An R^2 value was also generated via Excel (Fig 4.25.) for the purposes of assuring a well fitted trendline to the averaged raw data points.

It is then necessary to find the maximum amplitude of each of the trendline produced from the averaged data for each of the tested samples. This was accomplished using the aforementioned sixth order polynomial equations for each oil viscosity. The generated trendline equations were formatted to produce values to the 20th decimal place as to maintain accuracy. The generated equation was placed into a cell within excel. The "x variable" in each equation was replaced with the range of frequencies of the original frequency sweep. The maximum value of the resulting values was then found using the Excel "MAX()" function.

The average values were then multiplied by the vibrometer controller's displacement range setting of 5 micrometers/volt (5um/v) to convert the resonant amplitude values (provided in volts) to the actual displacement (micrometers (um)). The values for which can be seen (Table 4.2.-4.4.).

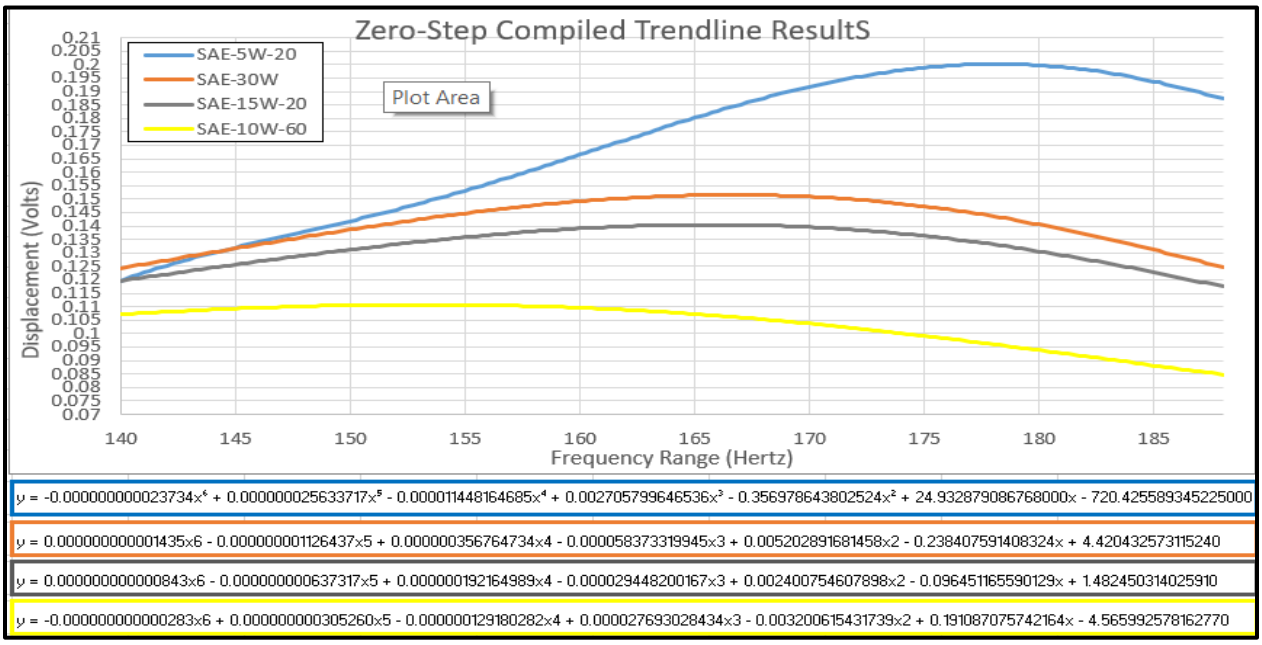

Figure 4.26: (Zero-Step) Compiled First Mode Resonant Frequency Amplitude (Laser position from clamping surface: x=12mm)

Measured Values (Freq. & Amp.)	Viscosity **(mPa*s)**	Resonant Frequency (Hz)	Amplitude (Volts)	R^2 Value	Amplitude (um)
Testing Sample					
10W-60	319.955	153.25	0.11077	0.99984	0.55385
15W-40	242.094	165.75	0.14048	0.99969	0.70240
0W-30	211.331	166.75	0.15159	0.99963	0.75797
5W-20	86.068	178.25	0.20020	0.99975	1.00100

Table 4.2: (Zero-Step) Compiled Numerical Data of (Figure 4.26)

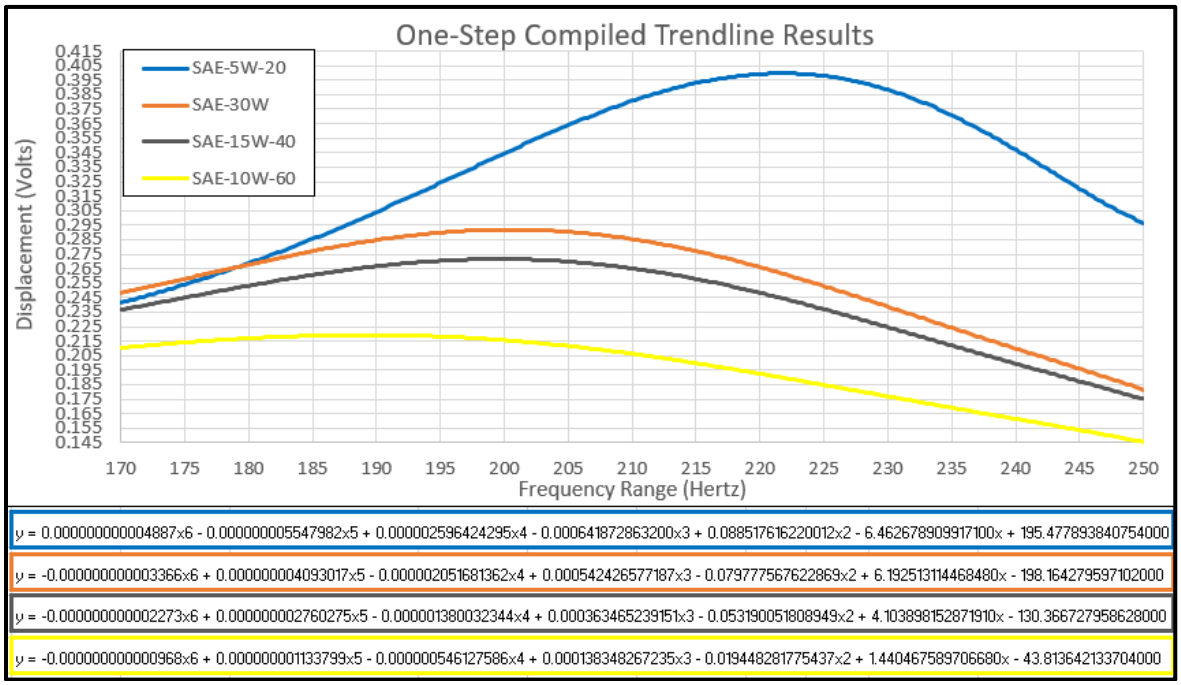

Figure 4.27: (One-Step) Compiled First Mode Resonant Frequency amplitude (Laser position from clamping surface: x=12mm)

Measured Values (Freq. & Amp.)	Viscosity **(mPa*s)**	Resonant Frequency (Hz)	Amplitude (Volts)	R^2 Value	Amplitude (um)
Testing Sample					
10W-60	319.9552	189.75	0.219239	0.9829	1.096
15W-40	242.0941	199.5	0.271594	0.9958	1.358
0W-30	211.3312	200.5	0.291938	0.9958	1.460
5W-20	86.067641	221.75	0.399704	0.9988	1.999

Table 4.3: (One-Step) Compiled Numerical Data of Figure (4.27)

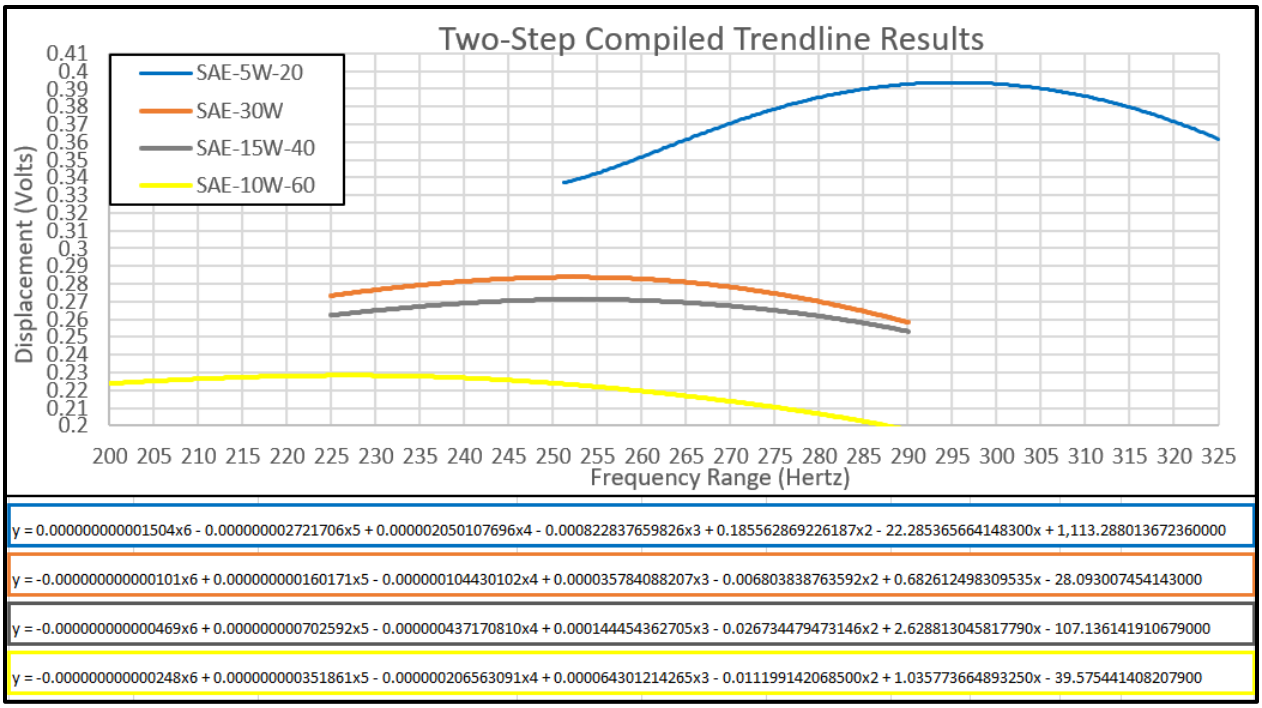

Figure 4.28: (Two-Step) Compiled First Mode Resonant Frequency amplitude (Laser position from clamping surface: x=12mm)

Measured Values (Freq. & Amp.)	Viscosity **(mPa*s)**	Resonant Frequency (Hz)	Amplitude (Volts)	R^2 Value	Amplitude (um)
Testing Sample					
10W-60	319.955	227.00	0.22834	0.98530	1.14172
15W-40	242.094	253.25	0.27128	0.99057	1.35642
0W-30	211.331	252.25	0.28382	0.99488	1.41912
5W-20	86.068	295.25	0.39370	1.00000	1.96849

Table 4.4: (Two-Step) Compiled Numerical Data of (Figure 4.28)

An analysis of the variation between the 4 runs for each testing fluid was also performed. The amplitude for each run was found individually and then averaged. The standard deviation between each of the four runs was calculated to ascertain the error (standard deviation) induced from the slight variation in maximum amplitudes between each run (Table 4.5.-4.7.). As can be

seen in (Table 4.5.-4.7.) the error between runs remained relatively low for all 3 cantilever designs, having a maximum error of only 1.273% of the maximum amplitude between them.

Run Number	AIR	SAE-5W-20	SAE-30W	SAE-15W-40	SAE-10W-60
Run1 (Volts)	1.460	0.200	0.153	0.142	0.111
Run2 (Volts)	1.490	0.200	0.152	0.141	0.111
Run3 (Volts)	1.500	0.201	0.151	0.140	0.111
Run4 (Volts)	1.500	0.200	0.151	0.140	0.111
Run Average	1.488	0.200	0.152	0.141	0.111
Standard Deviation	0.019	0.001	0.001	0.001	0.000
Percent Deviation	1.273	0.250	0.631	0.680	0.000

Table 4.5: (Zero-Step) Standard Deviation & Percent Deviation Calculation

Run Number	Air	SAE-5W-20	SAE-30W	SAE-15W-40	SAE-10W-60
Run1 (Volts)	0.405	0.405	0.295	0.273	0.220
Run2 (Volts)	0.401	0.401	0.297	0.271	0.220
Run3 (Volts)	0.397	0.397	0.296	0.271	0.219
Run4 (Volts)	0.396	0.396	0.291	0.271	0.219
Run Average	0.400	0.400	0.295	0.272	0.220
Standard Deviation	0.004	0.004	0.003	0.001	0.001
Percent Deviation	1.029	1.029	0.892	0.368	0.263

Table 4.6: (One-Step) Standard Deviation & Percent Deviation Calculation

Run Number	AIR	SAE-5W-20	SAE-30W	SAE-15W-40	SAE-10W-60
Run1 (Volts)	4.5	0.39400	0.28300	0.27200	0.22800
Run2 (Volts)	4.5	0.39400	0.28400	0.27100	0.22800
Run3 (Volts)	4.46	0.39500	0.28400	0.27200	0.22900
Run4 (Volts)	4.45	0.39300	0.28400	0.27100	0.22800
Run Average	4.47750	0.39400	0.28375	0.27150	0.22825
Standard Deviation	0.026	0.001	0.001	0.001	0.001
Percent Deviation	0.587	0.207	0.176	0.213	0.219

Table 4.7: (Two-Step) Standard Deviation & Percent Deviation

A “Percent Deviation” calculation was also performed. This calculation marks the percent difference between the run average and the standard deviation. This calculation serves to provide a basis for comparing the run-average standard deviation values for all tested fluids between all 3 cantilevers (Table 4.5.-4.7.).

Cantilever	Zero-Step	One-Step	Two-Step
Testing Sample			
SAE-10W-60	0	0.263	0.21905805
SAE-15W-40	0.68	0.368	0.212652033
SAE-30W	0.631	0.892	0.176211454
SAE-5W-20	0.25	1.029	0.207232635
Average	0.39025	0.638	0.203788543

Table 4.8: Percent Deviation Average Calculation

The average of the percent of change with reference to each cantilever was also calculated (Table 4.8.). This was done simply to ascertain a possible trend in the consistency between runs with regards to tip width. However, as can be seen in (Table 4.7) no such trend seems to exist. Possible reasons for this are discussed in (section 5.2).

The measured values were then plotted in Excel using a scatter plot (Fig 4.28.-4.30.). The scatter plots were then fitted with an exponential-type trendline. (Fig 4.28.-4.30.) displays the measured values after each had been converted to displacement values. The “R^2” value of (Fig 4.28.-4.30.) is a measure of the trendline fitment of the experimental data. As a value of “1” for an “R^2” represents a perfect fit, the indicated values in (Fig 4.28.-4.30.) show quite a good fit, thus helping to verify the measured values.

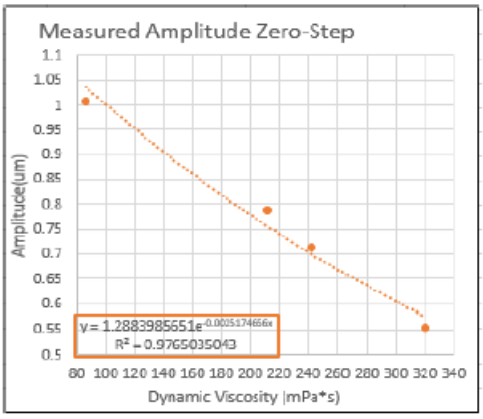

Figure 4.29: (Zero-Step) Measured Amplitude Graph

Percent Difference (Zero-Step)	Measured Values (um)	Trendline Values (um)	Percent Difference
Testing Sample			
SAE-10W-60	0.554	0.57575	3.95544
SAE-15W-40	0.702	0.70043	0.28101
SAE-30W	0.758	0.75683	0.15097
SAE-5W-20	1.001	1.03741	3.63788

Table 4.9: (Zero-Step) Trendline vs Measured Calculation

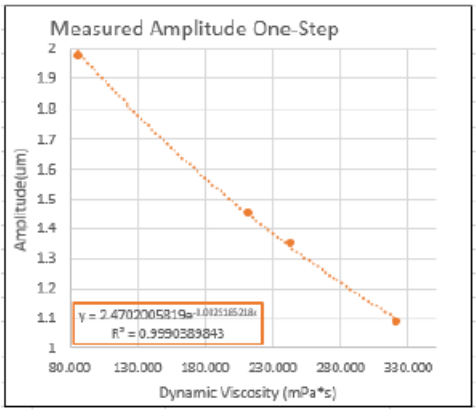

Figure 4.30: (One-Step) Measured Amplitude Graph

Percent Difference (One-Step)	Measured Values (um)	Trendline Values (um)	Percent Difference
Testing Sample			
10W-60	1.096	1.103	0.666
15W-40	1.358	1.343	1.135
0W-30	1.460	1.451	0.615
5W-20	1.999	1.989	0.486

Table 4.10: (One-Step) Trendline vs Measured Calculation

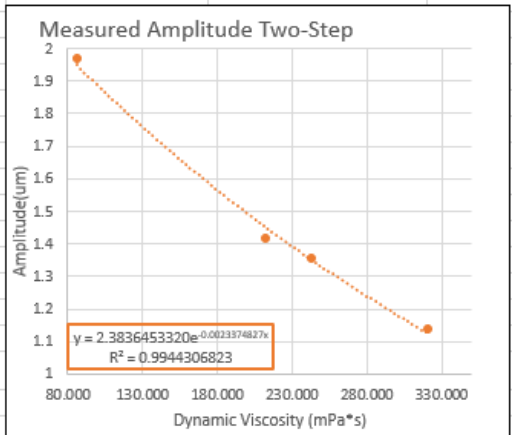

Figure 4.31: (Two-Step) Measured Amplitude Graph

Percent Difference (Two-Step)	Measured Values (um)	Trendline Values (um)	Percent Difference
Testing Sample			
10W-60	1.142	1.12833	1.17225
15W-40	1.356	1.35356	0.21089
0W-30	1.419	1.45448	2.49154
5W-20	1.968	1.94926	0.97691

Table 4.11: (Two-Step) Trendline vs Measured Calculation

Using the measured amplitude response values, it was now possible finish the theoretical calculation. The first step was to calculate the "N" values of (section 2.2). The results of which can be seen in (Table 4.12).

Testing Sample	Dynamic Viscosity (mPa*s)	Dynamic Viscosity (kg/mm*s)	Zero Step N value (m/s)	One Step N value (m/s)	Two Step N Value (m/s)
SAE-10W-60	319.955	0.000319955	0.679487244	1.078618767	1.712200565
SAE-15W-40	242.094	0.000242094	0.514134019	0.816136883	1.295536546
SAE-30	211.331	0.000211331	0.448803004	0.71243036	1.130912703
SAE-5W-20	86.068	8.60676E-05	0.182781414	0.290147409	0.460580303

Table 4.12: Theoretical Calculation (Obtaining N Value) Reference

NOTE: Values for "K", "N", and "Y" used to calculate "Q" are all taken from the highlighted row of (Table 4.12) SAE-10W-60.

Next, by comparing the measured trendline equations of (Fig 4.28.-4.30.) with (eq 2.11), the calibration coefficient "K" was determined by simply inserting the coefficient value of the measured trendline equation. Next the measured amplitude trendline value (Fig 4.28.-4.30.) was inserted for the "Y" value of the theoretical equation seen in (Table 4.13.).

	Zero-Step Cantilever	One-Step Cantilever	Two-Step Cantilever
Meaured Trendline Equation	$Y = 1.2883985651e^{-0.0025174666x}$	$Y = 2.4702005819e^{-0.0025185218x}$	$Y = 2.3836453320e^{-0.0023374827x}$
Theoretical Equation	$Y = K * e^{-N*Q}$		
N Value	−0.6794872444	−1.0786187666	−1.7122005649
K Value	1.2883985651	2.4702005819	2.3836453320
Y: (Amplitude From Measured Trendline Equation)	0.5757530144	1.1034980817	1.1283328882
Q (Calculated Value From Theoretical Equation)	1.1854200000	0.7470800000	0.4368000000

Table 4.13: Theoretical Calculation (Obtaining Q & K) Values Reference

NOTE: The "Q" and "K" values remained constant for every operating condition (Tested Sample).

The calibration coefficient "Q" was determined by setting (eq 2.11) with determined "K" value equal to measured trendline displacement value (um) from (Fig 4.28.-4.30.) along with

corresponding dynamic viscosity “N” value inserted into the theoretical equation and solving for “Q”.

	Zero-Step Cantilever	One-Step Cantilever	Two-Step Cantilever
Final Theoretical Equations	Amplitude (um) $= 1.2884e^{-N*0.8736}$	Amplitude (um) $= 2.4702 * e^{-N*0.5503}$	Amplitude (um) $= 2.3836 * e^{-N*0.3216}$

Table 4.14: Theoretical Calculation (Final Equations)

With the completed theoretical equation now derived, the calculated theoretical values along with measured values were plotted on the same graph for each cantilever (Fig 4.31.-4.33.).

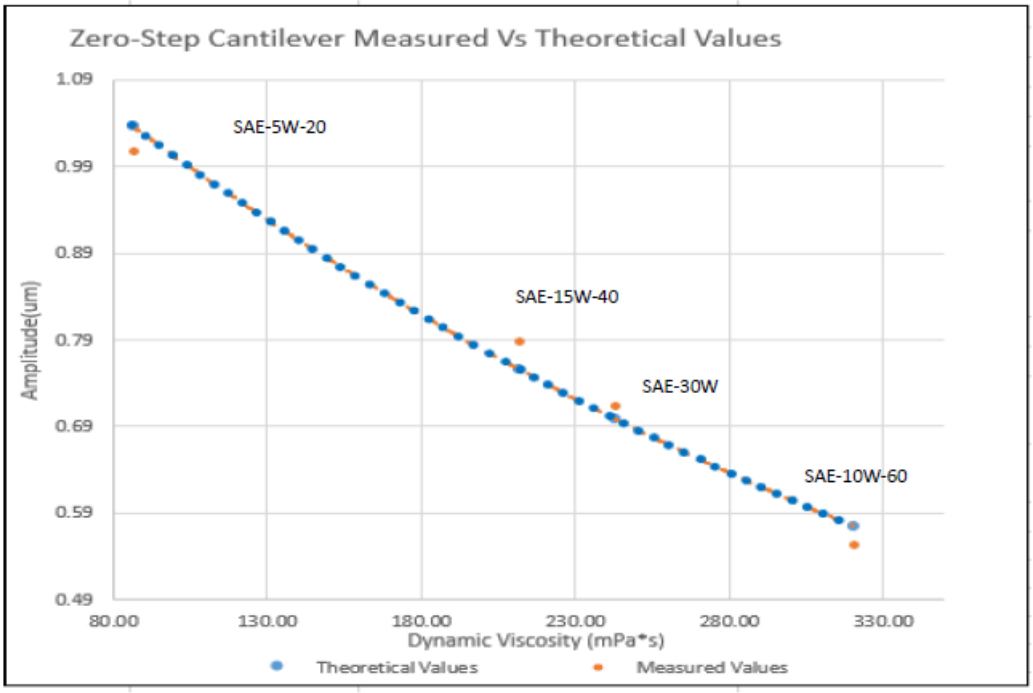

Figure 4.32: (Zero-Step) Measured and Theoretical Plotted Values and Trendline Fit

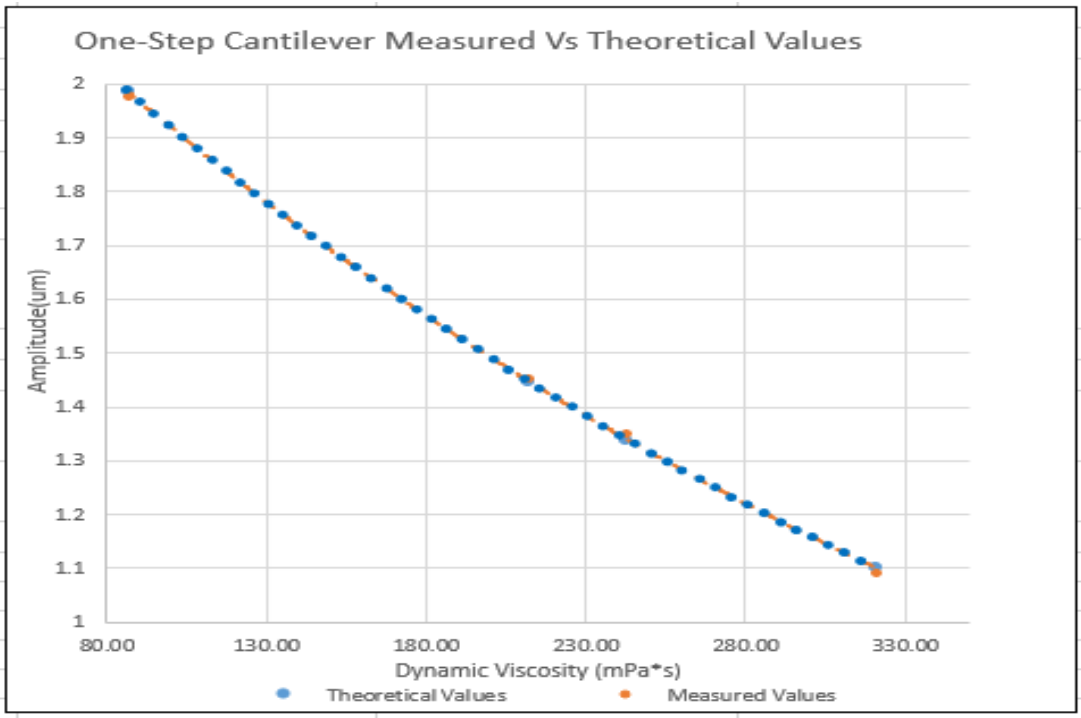

Figure 4.33: (One-Step) Measured and Theoretical Plotted Values and Trendline Fit

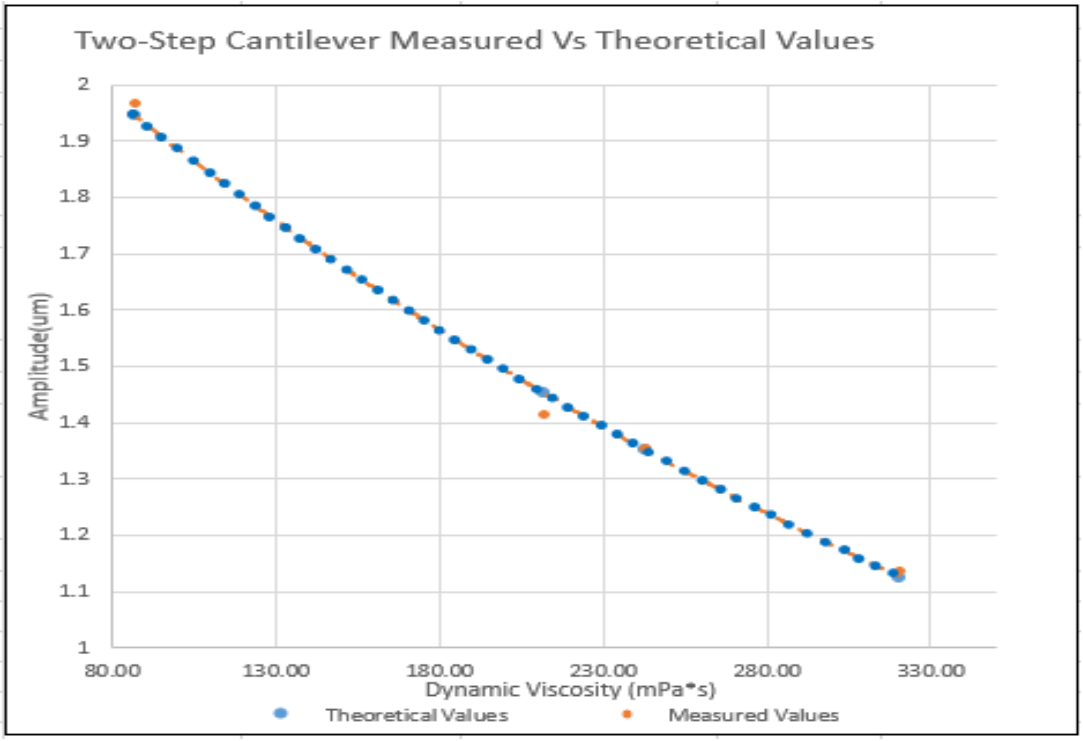

Figure 4.34: (Two-Step) Measured and Theoretical Plotted Values and Trendline Fit

As can be seen in (Fig 4.31.-4.33.). the theoretical (calculated) trendline and the measured trendline overlap virtually exactly. To verify this, trendline for each testing fluid are compared (Table 4.15.)

Tested Sample	SAE-10W-60	SAE-15W-40	SAE-30	SAE-5W-20
Trendline Theoretical Zero-Step	0.5757523	0.700427284	0.756827	1.0374101
Trendline Measured Value	0.57575301	0.700427941	0.756828	1.0374104
Amplitude Theoretical One-Step	1.10349768	1.342562112	1.450715	1.9888091
Trendline Measured Value	1.10349808	1.34256248	1.450716	1.9888093
Amplitude Theoretical Two-Step	1.1283335	1.353563311	1.45448	1.9492594
Trendline Measured Value	1.12833289	1.35356276	1.454479	1.9492591

Table 4.15: Theoretical Trendline Data Vs Measured Trendline Data

An additional goal of this research was to compare the sensitivity values of the three cantilever viscometers. However, due to time constraints caused by equipment failures only the Zero-Step data has been considered thus far. The sensitivity is calculated via (eq 4.1) below.

$$Sensitivity = \frac{Max\ Amplitude - Min\ Amplitude}{Max\ Viscosity - Min\ Viscosity} \qquad \text{Equation 4.1}$$

The sensitivity of the zero-step cantilever for both resonant frequency and amplitude measurements are shown in (Table 4.16-4.18). The resonant frequency the cantilever for each testing sample were calculated using the sixth order polynomial trendline equations of (Fig 4.25.-4.27.). The input amplitude values and results of this calculation can be seen in (Fig 4.22.). Note that the sensitivity values for resonant frequency and amplitude cannot be compared via this calculation as the ranges and reference values are very different.

Zero-Step Sensitivity Calculation	Viscosity **(mPa*s)**	Resonant Frequency (Hz)	Amplitude (um)
Oil Type			
10W-60	319.955	153.250	0.554
15W-40	242.094	165.750	0.702
0W-30	211.331	166.750	0.758
5W-20	86.068	178.250	1.001
Frequency Sensitivity:(Hz)/(mPa*s)			
Amplitude Sensitivity:(um)/(mPa*s)		0.10689	0.00191

Table 4.16: (Zero-Step) Sensitivity Calculation

One-Step Sensitivity	Viscosity **(mPa*s)**	Resonant Frequency (Hz)	Amplitude (um)
Testing Sample			
10W-60	319.955	189.750	1.096
15W-40	242.094	199.500	1.358
0W-30	211.331	200.500	1.460
5W-20	86.068	221.750	1.999
Frequency Sensitivity: (Hz)/(mPa*s) Amplitude Sensitivity: (nm)/(mPa*s)		0.13682	0.00386

Table 4.17: (One-Step) Sensitivity Calculation

Two-Step Sensitivity Calculation	Viscosity **(mPa*s)**	Resonant Frequency (Hz)	Amplitude (nm)
Oil Type			
10W-60	319.955	227.000	1.142
15W-40	242.094	253.250	1.356
0W-30	211.331	252.250	1.419
5W-20	86.068	295.250	1.968
Frequency Sensitivity:(Hz)/(mPa*s) Amplitude Sensitivity:(nm)/(mPa*s)		0.29181	0.00353

Table 4.18: (Two-Step) Sensitivity Calculation

Zero-Step Percent Change	Resonant Frequency (Hz)	Amplitude (um)
Oil Type		
SAE-10W-60	153.250	0.554
SAE-15W-40	165.750	0.702
SAE-30W	166.750	0.758
SAE-5W-20	178.250	1.001
Percent Change	16.31321	80.73534

Table 4.19: (Zero-Step) Amplitude vs. Frequency Response Comparison

One-Step Comparison Method	Resonant Frequency (Hz)	Amplitude (um)
Testing Sample		
10W-60	189.750	1.0962
15W-40	199.500	1.3580
0W-30	200.500	1.4597
5W-20	221.750	1.9985
Percent Change	16.86430	82.31435

Table 4.20: (One-Step) Amplitude vs. Frequency Response Comparison

Two-Step Comparison Method	Resonant Frequency (Hz)	Amplitude (nm)
Testing Samples		
10W-60	227.000	1.142
15W-40	253.250	1.356
0W-30	252.250	1.419
5W-20	295.250	1.968
Percent Change	30.06608	72.41489

Table 4.21: (Two-Step) Amplitude vs. Frequency Response Comparison

As there is no direct way to compare the sensitivity between the measured resonant frequency and amplitude values over the range of viscosities, another method was required. Therefore, the percent of change (POC) value was calculated using (eq 4.2) below.

$$\text{POC} = \left(\frac{\text{Difference between Highest and lowest measured value}}{\text{Highest Value}}\right) 100 \qquad \text{Equation 4.2}$$

A "percent of change" value indicates the percent increase/decrease between the highest and lowest values of a given range. As the range of measured values for frequency and amplitude are over the same range of viscosity values, percent change provides a reasonable method to compare resonant frequency to amplitude response. As can be seen from (Table 4.19.-4.21.) the amplitude response (POC) is consistently higher than the frequency response (POC).

As shown in (Table 4.22.) the amplitude (POC) reaches as almost high as 5 orders of magnitudes greater than the frequency (POC).

Cantilever	Frequency (Percent of Change)	Amplitude (Percent of Change)	(Amplitude POC)/(Frequency POC)
Zero-Step Percent of Change	16.3132	80.7353	4.9491
One-Step Percent of Change	16.8643	82.3144	4.8810
Two-Step Percent of Change	30.0661	72.4149	2.4085

Table 4.22: Amplitude (POC)/Frequency (POC)

Using the completed analytical calculation, graphs were extrapolated over a wider range of values (Fig 4.34.-4.36.). The data displayed in (Fig 4.34.-4.36.) is over a wider projected range of viscosity values that what was experimentally measured. From the graphs, one should be able

to determine the viscosity of an unknown fluid based on the measured displacement amplitude of the microcantilever viscometer over the projected range.

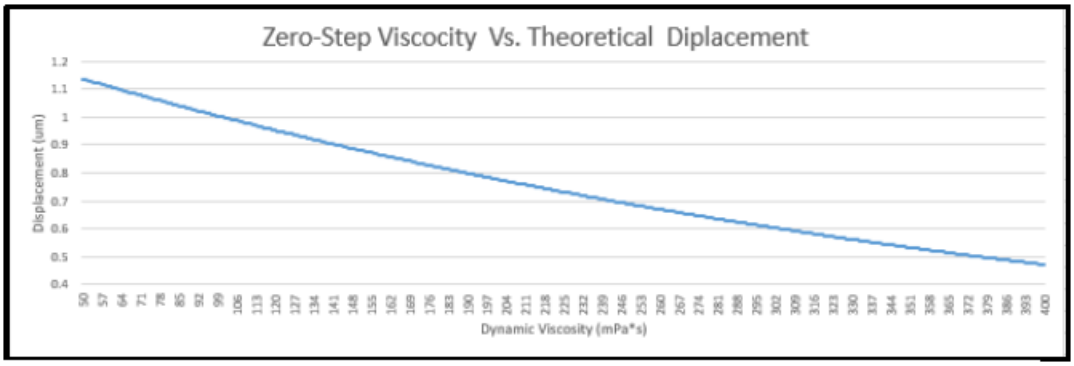

Figure 4.35: (Zero-Step) Theoretical Viscosity Vs Amplitude Extrapolation

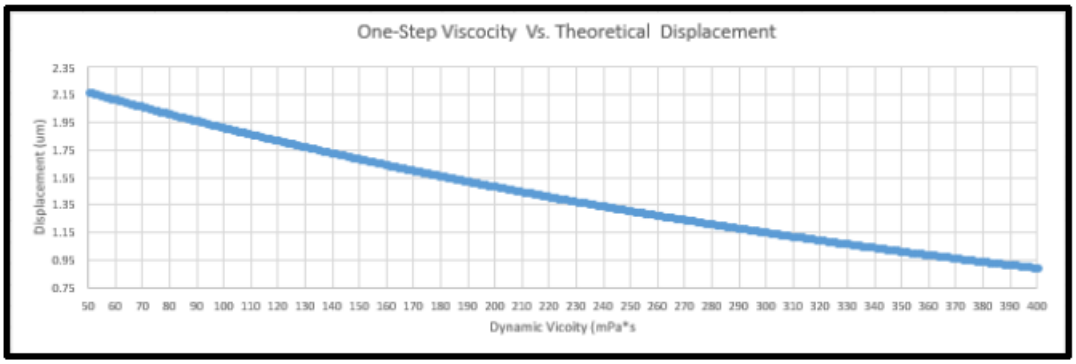

Figure 4.36: (One-Step) Theoretical Viscosity Vs Amplitude Extrapolation

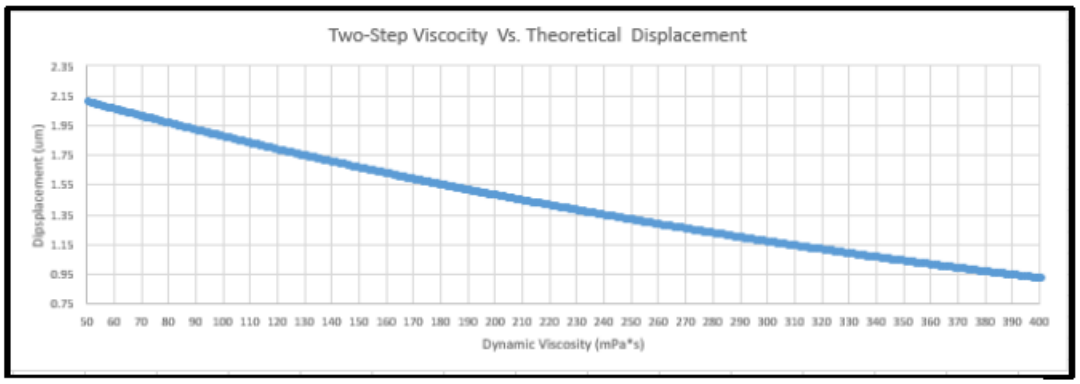

Figure 4.37: (Two-Step) Theoretical Viscosity Vs Amplitude Extrapolation

4.9 Additional Analysis

Further analysis was performed in addition to the itemized scope of this project. Firstly, the plotted measured amplitude response values were evaluated with logarithmic along with a

linear regression as to ascertain if the "R^2" values will present a better fit than the polynomial regression previously presented.

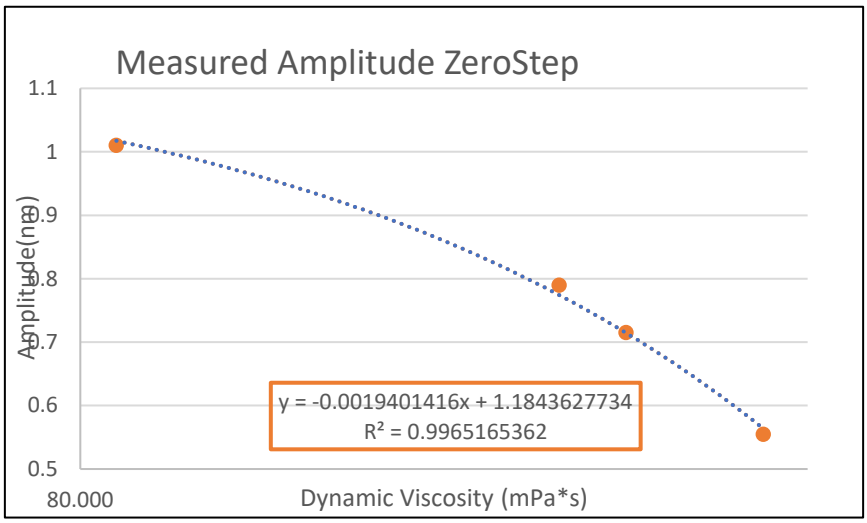

Figure 4.38: (Zero-Step) Logarithmic (x-axis) and linear regression.

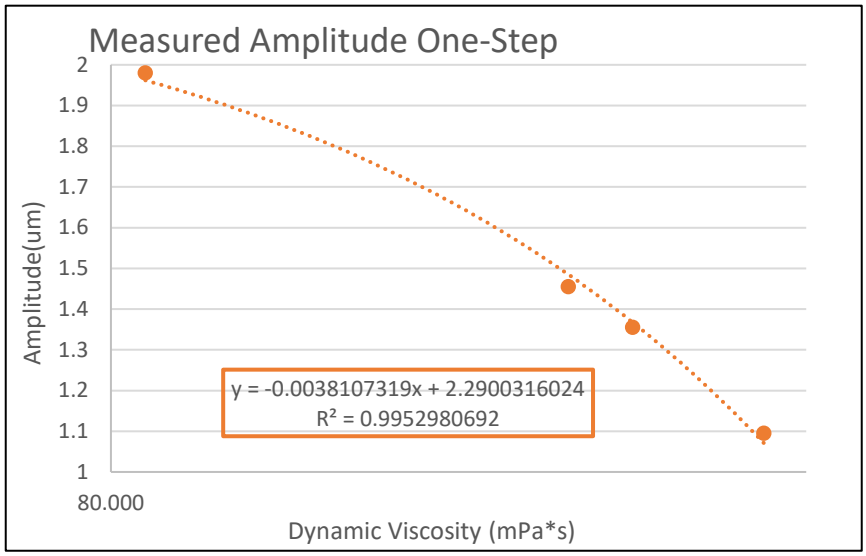

Figure 4.39: (One-Step) Logarithmic (x-axis) and linear regression.

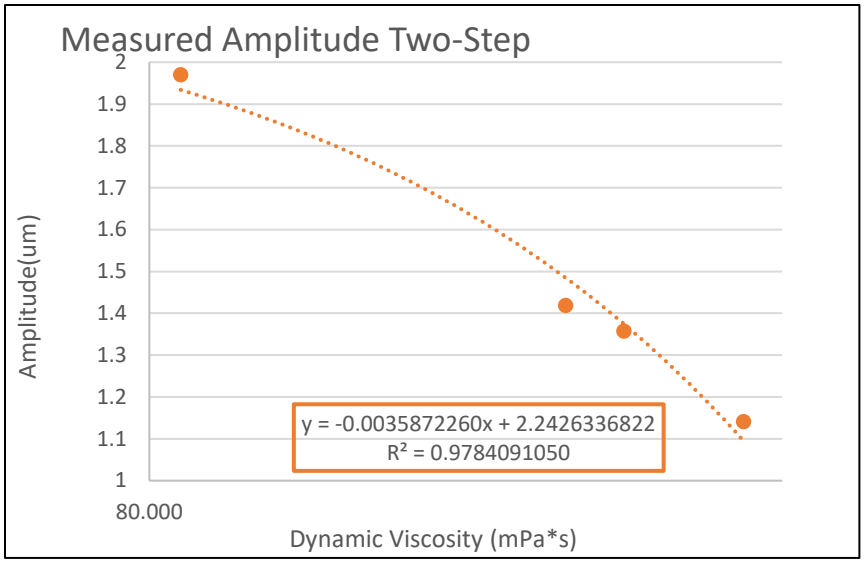

Figure 4.40: (Two-Step) Logarithmic (x-axis) and linear regression.

(Fig 4.37.-4.39.) Show the measured displacement values with a logarithmic (x-axis) and a liner regression. Unfortunately, upon analyzing the "R^2" values, it appears to have a slightly worse "fit" as it were when compared to the initial method (Fig 2.28.-2.30.). Therefore, this may not a viable method of analysis.

Each of the 3 cantilevers were also tested for sensitivity at different immersion depths. As it was easier to take new readings rather than spend the time iteratively to set the laser position, immersion depth, and clamping position exactly as they were in the previous experiments, all new results were taken for the 4mm immersion depth. However, as can be seen in (Fig 4.37.-Fig4.39.) the 4 mm amplitude measurements were quite close to previous results.

Zero-Step Sensitivity Calculation	Viscosity **(mPa*s)**	4mm insertion	3mm insertion	2mm insertion
Oil Type				
10W-60	319.96	0.131	0.152	0.233
5W-20	86.07	0.258	0.301	0.48
Amplitude Sensitivity:(um)/(mPa*s)		0.00054	0.00064	0.00106

Figure 4.41: (Zero-Step) Depth Sensitivity Analysis

One-Step Sensitivity Calculation	Viscosity (mPa*s)	4mm insertion	3mm insertion	2mm insertion
Oil Type				
10W-60	319.96	0.216	0.26	0.31
5W-20	86.07	0.385	0.427	0.565
Amplitude Sensitivity:(um)/(mPa*s)		0.00072	0.00071	0.00109

Figure 4.42: (One-Step) Depth Sensitivity Analysis

Two-Step Sensitivity Calculation	Viscosity (mPa*s)	4mm insertion	3mm insertion	2mm insertion
Oil Type				
10W-60	319.96	0.239	0.263	0.395
5W-20	86.07	0.408	0.506	0.81
Amplitude Sensitivity:(um)/(mPa*s)		0.00072	0.00104	0.00177

Figure 4.43: (Two-Step) Depth Sensitivity Analysis

(Fig 4.40.-Fig 4.42.) show the sensitivity calculations measured at 4mm, 3mm, and 2mm insertion. The Sensitivity seemed to show a general increase as insertion depth decreased. The difference between the SAE-10W-60 amplitude and the SAE-5W-20 amplitude increased as insertion depth decreased.

4.10 Considerations for Error

Throughout the experiment it was necessary to recognize possible sources of error that may have contributed and effected the results. The ambient room temperature during varied during the day by +/- 0.5-degree Celsius. The 23-degree Celsius measurement used for calculating the viscosity for the theoretical calculation may have slightly changed during the course of the experiment. However, all the testing samples were stored within 8 inches of each other and in the same type of test tubes. Therefore, as the amount of each sample was the same in

each test tube any variation in room temperature would affect the samples equally. As the calibration coefficients “Q” and “K” were used in the analytical calculation any deviation would be accounted for. If the temperature in the room had decreased slightly before the experimentation was performed, this samples would have cooled down the relatively equally. As these tests were performed during the late afternoon/night during the summer months, it is feasible that the temperature in the room had decreased slightly from earlier in the day.

It is worth noting that the intended dimensions for the three cantilevers were slightly askew. Due to the method by which the cantilevers were cut (CNC Laser) the cantilevers grew by about 5.5%. The CNC Laser cutting process may have also affected the Young’s Modulus of the stainless steel used to make the cantilevers. However, as the calibration coefficients “Q” and “K” were used in the analytical calculation any dimensional deviation was compensated for and therefore won’t affect the results of the calculations. However, if this experiment is to be repeated by another party, these factors may influence duplication of the experimental results.

After performing the experiments, the realization that the height of the capillary action of the oil may be significantly affected by the oil’s viscosity/density. As the top edge of the capillary action of the oil samples was used as the insertion depth reference, this may have affected the results. Further study regarding the capillary affect is necessary to determine the significance of this affect.

The intended dimensions for the PZT-5Hs were slightly different than intended. As the new piezo had been initially cut using the CNC Laser cutter, most of the area of the piezo sample had been destroyed. The peizos used in the experiment were fabricated from the (off-cuts) from the CNC laser cutting process. Due to this they could not be made exactly to size.

The deviations between experimental runs could have been caused by any induced

“noise” from external sources of vibration. As the experiments were performed on a scientific lab table with passive vibration only, any significant ground vibration would have introduced vibration. Other sources include ambient room noise/sounds as well as any air currents.

CHAPTER 5

CONCLUSION

5.1 Conclusion from Results

In this research, analytical modeling as well as experimental analysis for the amplitude response of a vibrating cantilever with viscous tip drag as it applies to viscosity measurement has been presented. The effects of varying viscous drag forces on the tip of 3 different vibrating cantilever designs were observed as it applied to amplitude response. Analytical calculation were also performed to find a correlation between dynamic viscosity and vibrational amplitude. The analytical calculations were derived from the Euler-Bernoulli beam equation. A version of Stokes-Law was used in the beam equation to account for the effects of viscous drag force. The analytical calculation made allowances for calibration to the experimental data via two calibration coefficients built into the final equation. An FEA simulation was also performed using ComSol as to ascertain the first-mode resonant frequency values of each cantilever while vibrating in a vacuum. The FEA calculation served to provide a maximum possible resonant frequency value for each cantilever from which the viscously dampened resonant frequency required for experimentation will reside below.

The overall objective of this research was to provide experimental evidence as to the viability of determining viscosity via an oscillating microcantilever partially immersed in a testing fluid by measuring amplitude response. The results of the experimental data clearly show a consistent exponential trend relating amplitude response to dynamic viscosity. The minimal variation between the four different runs for each of the four testing samples clearly demonstrates a consistent amplitude response due to dynamic viscosity for all 3 cantilevers. An additional comparison of the viscous effects between frequency and amplitude response clearly

shows amplitude response as the more sensitive measurement value. An additional study was performed to test sensitivity as it applies to immersion depth. The results suggest that a minimal insertion depth will result in the greatest sensitivity to dynamic viscosity for all 3 cantilever viscometers.

5.2 Future Work

Fabrication of the microcantilever via machining instead of CNC laser cutting would reduce dimensional inaccuracy due to thermal expansion. It would also prove to be useful to have an alternative viscometer as to determine the exact viscosity of the testing sample before running the experimentation. Lastly, testing the cantilevers over a greater range of viscosities would serve to further verify the theoretical amplitude response. Developing a viscometer design using a piezo to measure amplitude response in leu of the laser vibrometer is the next important step for creating a commercial product based on the research discussed in this paper.

REFERENCES

[1] N. Genrikh, V & Kaplun, A & N. Solovev, A. (1972). Study of Liquid Viscosity by Means of Vibration Method. 42.

[2] "Determining Resonance Frequency | Piezo Theory." APC International Ltd, www.americanpiezo.com/knowledge-center/piezo-theory/determining-resonance-frequency.html.

[4] "Piezoelectric Materials: Crystal Orientation and Poling Direction." COMSOL, www.comsol.com/blogs/piezoelectric-materials-crystal-orientation-poling-direction/.

[5] Dineva, Petia, et al. "Dynamic Fracture of Piezoelectric Materials." Solid Mechanics and Its Applications, 2014, doi:10.1007/978-3-319-03961-9.

[6] Shih, Wan Y., et al. "Simultaneous Liquid Viscosity and Density Determination with Piezoelectric Unimorph Cantilevers." Journal of Applied Physics, vol. 89, no. 2, 2001, pp. 1497–1505., doi:10.1063/1.1287606.

[7] Salgar, Mr. Manojkumar Madhukar. "Dynamic Modeling of AFM Cantilever Probe Under Base Excitation system A thesis submitted in partial fulfillment of the requirements for the degree of Master of Technology in Machine Design and Analysis by Mr ." (2013).

[8] Sathiya, S., and B. Vasuki. "A Structural Tailored Piezo Actuated Cantilever Shaped 2-DOF Resonators for Viscosity and Density Sensing in Liquids." Sensors and Actuators A: Physical, vol. 247, 2016, pp. 277–288., doi:10.1016/j.sna.2016.05.052.

[9] Eris, Gamze, et al. "Determination of Viscosity and Density of Fluids Using Frequency Response of Microcantilevers." The Journal of Supercritical Fluids, vol. 105, 2015, pp. 179–185., doi:10.1016/j.supflu.2015.04.012.

[10] Wang, Gang, et al. "A Contact Resonance Viscometer Based on the Electromechanical Impedance of a Piezoelectric Cantilever." Sensors and Actuators A: Physical, vol. 267, 2017, pp. 401–408., doi:10.1016/j.sna.2017.10.041.

[11] "Viscosity of Engine Oil – Viscosity Table and Viscosity Chart :: Anton Paar Wiki." Anton Paar, wiki.anton-paar.com/en/engine-oil/.

[12] Riesch, Christian, et al. "Characterizing Vibrating Cantilevers for Liquid Viscosity and Density Sensing." Journal of Sensors, vol. 2008, 2008, pp. 1–9., doi:10.1155/2008/697062.

[13] Boskovic, S., et al. "Rheological Measurements Using Microcantilevers." Journal of Rheology, vol. 46, no. 4, 2002, p. 891., doi:10.1122/1.1475978.

[14] "Viscometer." Bitao's Research Group - In SNST, Lanzhou University, snst-hu.lzu.edu.cn/zhangyi/ndata/Viscometer.html.

[15] "Absolute, Dynamic and Kinematic Viscosity." Densities of Solids, www.engineeringtoolbox.com/dynamic-absolute-kinematic-viscosity-d_412.html.

[16] "Types of Viscosity Measurement Devices: Viscometers and Rheometers." Brighthub Engineering, 24 Aug. 2010, www.brighthubengineering.com/fluid-mechanics-hydraulics/83996-viscosity-measurement-equipment/.

[17] "Viscometers." Visual Encyclopedia of Chemical Engineering, encyclopedia.che.engin.umich.edu/Pages/ProcessParameters/Viscometers/Viscometers.html.

[18] Process, Lab &. Lab & Process | Norcross Viscosity Controls, www.labandprocess.com/en/referenced_companies/norcross-viscosity-controls.

[19] "Gardco :: Viscosity Tubes." Gardco :: EZ Zahn Viscosity Cups, www.gardco.com/pages/viscosity/vi/bubble_viscometers.cfm.

[20] "Viscometer." Wikipedia, Wikimedia Foundation, 19 June 2018, en.wikipedia.org/wiki/Viscometer.

[21] HYSEN :::www.hysen.com/product/view.php?idx=3&no=3&cat_no=&offset.

[22] "Controllori." BPS Srl, www.bpsweb.it/polytec/vibrometri-laser/modulare-ofv/controllori/.

[23] Thingiverse.com. "Platform Jack [Fully Assembled, No Supports] by Intentional3D." By Jett0312 - Thingiverse, www.thingiverse.com/thing:925556.

[24] Hughes, Matt. "Matt Hughes - President - Semicore Equipment, Inc." Semicore, www.semicore.com/news/89-what-is-e-beam-evaporation.

[25] "Piezoelectricity." Wikipedia, Wikimedia Foundation, 26 June 2018, en.wikipedia.org/wiki/Piezoelectricity.

[26] Sumali, Hartono & Carne, Thomas. (2008). Air-drag damping on micro-cantilever beams. Conference Proceedings of the Society for Experimental Mechanics Series.

[27] David Leith (1987) Drag on Nonspherical Objects, Aerosol Science and Technology, 6:2, 153-161, DOI: 10.1080/02786828708959128

[28] Tichý*, Jan, et al. "Piezoelectric Properties." Fundamentals of Piezoelectric Sensorics, 2010, pp. 69–100., doi:10.1007/978-3-540-68427-5_5.

[29] "You Are Here:" LubeDB - Oils, Greases, Petrochemicals Database, lubebase.com/cgi-bin/ctl/lube/EXXON-Superflo-5W20?id=4166.

[30] Matthew, Paul. “C2.2 Composite Beams.” Engineering Core Courses, www.engineeringcorecourses.com/solidmechanics2/C2-bending/C2.2-composite-beams/theory/.

[31] “Piezo Basics.” CTS, www.ctscorp.com/resource-center/tutorials/piezo-basics/.

[32] Roaten, David. “Pearl Cutting Saw.” Stewart-MacDonald Guitar Tools Parts Supplies, 5 Mar. 2018, www.stewmac.com/Luthier_Tools/Types_of_Tools/Saws/Pearl_Cutting_Saw.html?utm_source=google&utm_medium=shopping&utm_campaign=2018-07-gp&gclid=CjwKCAjwg_fZBRAoEiwAppvp-bITp50-BdSO9xYp6NcqZuswQqlWJ093hOveiCpqbQ5367trvCQAKBoCkWgQAvD_BwE.

[33] “Boston Piezo-Optics Inc.” *Boston Piezo Optics Inc.*, www.bostonpiezooptics.com/.

[34] “Dielectric.” *Wikipedia*, Wikimedia Foundation, 16 July 2018, en.wikipedia.org/wiki/Dielectric.

[35] “Viscometers.” *Visual Encyclopedia of Chemical Engineering*, encyclopedia.che.engin.umich.edu/Pages/ProcessParameters/Viscometers/Viscometers.html.